

SPECTROSCOPY OF KISS EMISSION-LINE GALAXY CANDIDATES. I. MDM OBSERVATIONS

GARY WEGNER

Department of Physics and Astronomy, 6127 Wilder Laboratory, Dartmouth College, Hanover, NH 03755; Gary.Wegner@dartmouth.edu

AND

JOHN J. SALZER, ANNA JANGREN, CARYL GRONWALL,¹ AND JASON MELBOURNE²

Astronomy Department, Wesleyan University, Middletown, CT 06459; slaz@astro.wesleyan.edu, anna@astro.wesleyan.edu

Received 2002 December 30; accepted 2003 February 5

ABSTRACT

Spectroscopic observations for 351 emission-line galaxy candidates from the KPNO International Spectroscopic Survey (KISS) have been obtained using the MDM Observatory 2.4 m telescope on Kitt Peak. KISS is an ongoing wide-field objective-prism survey for extragalactic emission-line objects, which has cataloged over 2200 emission-line galaxy (ELG) candidates to date. Spectroscopic follow-up observations are being carried out to study the characteristics of the survey objects. The observational data presented here include redshifts, reddening estimates, line equivalent widths, $H\alpha$ line fluxes, and emission-line ratios. The galaxies have been classified based on their emission-line characteristics. The procedure for selecting the ELG candidates in KISS is found to be very reliable: 95% of the candidates in this sample are verified to have emission lines. A comparison of objective-prism survey data—redshifts, $H\alpha$ line fluxes, and equivalent widths—with the long-slit measurements shows good overall agreement.

Key words: galaxies: Seyfert — galaxies: starburst — surveys

1. INTRODUCTION

The KPNO International Spectroscopic Survey (KISS) is an objective-prism survey designed to provide basic observational data for a large number of extragalactic emission-line sources. The survey is being carried out with the 0.61 m Burrell Schmidt telescope³ at Kitt Peak. The use of a CCD detector distinguishes this survey from the classical photographic objective-prism surveys, allowing us to probe much fainter flux levels. To date, we have identified 2271 emission-line objects. The specific details of the survey have been described in the first paper in the KISS series (Salzer et al. 2000, hereafter Paper I). The first three survey lists are presented in Salzer et al. (2001, hereafter KR1), Salzer et al. (2002, hereafter KB1), and in Gronwall et al. (2003b, hereafter KR2). In this paper, we concentrate on the spectroscopic properties found for a subsample of the survey sources. The spectroscopic properties of the full sample of KISS emission-line galaxies (ELGs) will be presented in future papers (Gronwall et al. 2003a; Chomiuk, Salzer, & Gronwall 2003).

Members of the KISS group have obtained long-slit spectra of KISS ELG candidates at several telescopes. To date, we have obtained follow-up spectroscopy for 1052 of the ELG candidates, or nearly half of the survey sample. These observations allow us to explore the properties of the KISS emission-line objects in greater detail. This is the first in a series of papers that will present slit spectral data for large numbers of KISS ELGs. This paper presents the largest

sample of follow-up spectra acquired to date: the data obtained for 351 objects over four seasons at the MDM 2.4 m telescope. The results from observations at other telescopes will be presented in future papers (e.g., Melbourne et al. 2003; Salzer et al. 2003). In addition to tabulating the spectral data, we also use the MDM spectroscopic results for a comparison with the properties derived from the objective-prism survey data listed in the KISS catalogs. In § 2, we describe the selection of the sample, the observations, and the data reduction. The properties measured in the long-slit spectra are presented in § 3, and in § 4 we compare these with the corresponding survey database properties. We present our conclusions in § 5.

2. OBSERVATIONS

We obtained spectra for 351 KISS objects at the MDM 2.4 m telescope over the course of four observing runs in 1998 May, 1999 April, 2000 May, and 2001 March. Details of the observing runs are listed in Table 1. Column (1) lists the dates of the observations, and column (2) gives their run identification numbers, which are used for internal record keeping. The last digit indicates which night during a given observing run the observations were obtained, and the preceding digit(s) denote the number of the observing run in our program of follow-up spectroscopic observations (e.g., run ID = 152 designates night 2 of KISS follow-up spectroscopy run number 15). Column (3) indicates the sky conditions during the night, and column (4) lists the number of follow-up spectra that were obtained.

2.1. Sample Selection

The galaxies selected for follow-up spectroscopy at MDM were in most cases not chosen at random from the survey lists. Rather, the galaxies chosen were often observed in support of a specific project being done by members of the KISS team at the time of the observing run. Since the

¹ Current address: Department of Astronomy and Astrophysics, Pennsylvania State University, University Park, PA 16802; caryl@astro.psu.edu.

² Current address: Department of Astronomy and Astrophysics, University of California, Santa Cruz, 1156 High Street, Santa Cruz, CA 95064; jmel@ucolick.org.

³ The Burrell Schmidt telescope is part of the Warner and Swasey Observatory, Case Western Reserve University.

TABLE 1
MDM SPECTROSCOPIC OBSERVING RUNS

Date (1)	Run ID (2)	Conditions (3)	Number Observed (4)
1998 May 2	21	Clear, good spectrophotometry	28
1998 May 3	22	Clear, good spectrophotometry	36
1998 May 4	23	Variable clouds	31
1999 Apr 21....	31	Clouds early, then clear	40
1999 Apr 22....	32	Clear, good spectrophotometry	41
2000 May 24...	111	Clear, good spectrophotometry	39
2000 May 25...	112	Mostly clear, cloudy at end of night	35
2001 Mar 20 ...	151	Clouds early, then clear	16
2001 Mar 21 ...	152	Clouds early, then clear	41
2001 Mar 22 ...	153	Clear, good spectrophotometry	44

precise sample selection can shape significantly the characteristics of the galaxies presented in the current paper (e.g., fraction of AGNs vs. star-forming galaxies), we detail here the contents of the observing lists used during each season of MDM observations.

During the first year of spectroscopic follow-up (1998), our primary goal was to establish the properties of a random sample of KISS ELG candidates and to assess the adequacy of our objective-prism selection methods. Therefore, our primary observing lists included complete sampling of specific survey fields. We managed to observe nearly all KISS candidates in two fields (F1305 and F1610; see § 3.3), as well as roughly half of the objects in two other fields (F1415 and F1520). We also wished to explore the properties of the most extreme KISS objects, so we observed a subsample of objects with the highest $H\alpha$ luminosities (as estimated from the objective-prism redshifts and fluxes). Many of these latter objects turned out to be AGNs.

During the 1999, 2000, and 2001 MDM observations, our main focus was on observing KISS galaxies that were also included in one or more other wide-field surveys carried out at nonoptical wavelengths. For example, in 1999 our main observing list included objects from the KR1 catalog that were also detected in the FIRST radio continuum survey (Becker, White, & Helfand 1995; White et al. 1997). In 2000, the follow-up observations of KISS ELGs in FIRST was expanded to include objects in KR2 and also added *IRAS* far-infrared-detected ELGs as well (Moshir, Kopman, & Conrow 1992). We also observed galaxies selected as being of lower redshift (again, based on the objective-prism estimate), in support of a project to obtain $H\text{ I } 21\text{ cm}$ observations of nearby dwarf ELGs at Arecibo Observatory. In 2001, many KISS ELGs included in either the NVSS radio survey (Condon et al. 1998) or the *ROSAT* All-Sky Survey (Voges et al. 1999) were observed. In addition, during the 2001 season, we also selected galaxies from a list that included all galaxies with absolute magnitudes above $M_B = -19.5$, with the goal of gaining complete observations of the more luminous portion of the KISS sample. Finally, we began systematic observations of the [O III]-selected KISS galaxies (KB1) in 2001 as well. Papers detailing the results of some of the multiwavelength studies have already been published (Stevenson et al. 2002 for the *ROSAT*-KISS study; Lee et al. 2002 for the $H\text{ I}$ study) or are in an advanced stage of preparation (e.g., Van Duyne et al. 2003 for the FIRST-NVSS radio project).

As a result of our method of sample selection, we preferentially observed objects that were among both the most luminous and least luminous galaxies in the KISS sample. In addition, the radio- and X-ray-selected samples contain more AGN than would be expected from a randomly selected sample. Hence the proportion of AGNs found in the MDM-observed sample is quite high (see § 3.2). Comparison of the characteristics of the current list of MDM-observed KISS ELGs with other galaxy samples must keep these sample selection issues in mind.

2.2. Instrument Setup

All observations were taken with the Mark III Spectrograph, using a slit width of $1''.68$. The grating used had 300 grooves mm^{-1} and was blazed at 5400 Å, giving a reciprocal dispersion of $5.4\text{ \AA pixel}^{-1}$. The spectral range covered was 4000–8500 Å. On some of the earlier runs, spectra with coverage up to 9000 Å were obtained; emission lines at the extreme red end were not well focused, and we did not use them to determine object redshifts. Different detectors were used on different runs; all had similar spectral response and the same pixel size, yielding a pixel scale along the slit of $0''.78\text{ pixel}^{-1}$. Exposure times ranged from 2 to 20 minutes. Each night of observations included images of a HgNe lamp to set the wavelength scale, images where the CCD was illuminated by a quartz flat-field lamp, and images of several spectrophotometric standard stars for flux calibration.

2.3. Data Reduction

The data reduction was carried out with the Image Reduction and Analysis Facility (IRAF).⁴ Processing of the two-dimensional spectral images followed standard methods. The mean bias level was determined from the overscan region of each image and subtracted from the image. For each night, 10 zero-second exposures were average-combined to create a mean bias image, which was subtracted to correct the science images for any possible two-dimensional structure. To achieve flat fielding, we used a median-combined quartz lamp image that had been corrected for wavelength-dependent response.

One-dimensional spectra were extracted using the IRAF routine APALL in the APEXTRACT package. The extraction width (i.e., distance along the slit) was selected independently for each source by running APALL interactively. For most sources, the emission region was unresolved spatially, so that the extraction width was limited to $\sim 5''\text{--}7''$. This extraction region typically included greater than 90% of the observed emission-line flux for each object.

Sky subtraction was also performed at this stage, with the sky spectrum being measured in $35''\text{--}40''$ wide regions on either side of the object. The HgNe lamp spectra were used to assign a wavelength scale, and the spectra of the spectrophotometric standard stars were used to establish the flux scale. The standard-star data were also used to correct the spectra of our target ELGs for telluric absorption. This is important for our ELGs, since for certain redshifts lines like the [S II] doublet, [N II], or $H\alpha$ could fall in the strong *B* band and lead to a severe underestimate of the true line flux.

⁴ IRAF is distributed by the National Optical Astronomy Observatory, which is operated by the Association of Universities for Research in Astronomy, Inc., under cooperative agreement with the National Science Foundation.

The emission-line fluxes and equivalent widths were measured using the SPLOT routine in the ONEDSPEC package.

The resolution of the MDM spectra does not fully separate the $H\alpha$ and $[N\text{ II}]\lambda 6583$ lines. We measured the total flux of the blended line complex, the flux ratio of the peaks of the $H\alpha$ and $[N\text{ II}]$ lines, and the line positions. Based on these data, we then separated the lines with a deblending routine to determine the $H\alpha$ flux and the $[N\text{ II}]/H\alpha$ ratio. In a few cases, the $[N\text{ II}]$ line was too weak to be visible, except as a broadened “wing” on the red side of $H\alpha$; we did not attempt to deblend the lines in such objects.

The decimal reddening coefficient $c_{H\beta}$ (defined in eq. [1]) was calculated based on the measured ratio of $H\alpha$ to $H\beta$ flux, assuming an intrinsic ratio of 2.86 and an electron temperature of $T_e = 10,000$ K. If the $[O\text{ III}]\lambda 4363$ line flux was measured, the dereddening program used this to iterate a new value for both T_e and the intrinsic $H\alpha/H\beta$ ratio. The measured line ratios were then corrected for reddening using $c_{H\beta}$, following the standard prescription (e.g., Osterbrock 1989):

$$\frac{I(\lambda)}{I(H\beta)} = \frac{F(\lambda)}{F(H\beta)} \exp[c_{H\beta}f(\lambda)], \quad (1)$$

where f has been measured from studies of absorption in the Milky Way. For 10 objects, the measured $H\alpha/H\beta$ ratio yields a negative value for $c_{H\beta}$. In the majority of these cases, the formal error in $c_{H\beta}$ is such that the measured value is consistent with $c_{H\beta} = 0.00$. Whenever a negative $c_{H\beta}$ was measured, $c_{H\beta} = 0.00$ was used for the computation of reddening-corrected line ratios. The measured (negative) $c_{H\beta}$ values are listed in the tables.

3. KPNO INTERNATIONAL SPECTROSCOPIC SURVEY: LIST OF MDM FOLLOW-UP SPECTROSCOPY

3.1. Spectroscopic Data

The results of our spectroscopic observations of the MDM sample are presented in Tables 2, 3, and 4. The tables are organized by the KISS source catalogs in which the targets are located. Table 2 lists the spectral data for KISS ELGS from the first red survey list (30° Red Survey; KR1), Table 3 presents the results for objects from the second red survey list (43° Red Survey; KR2), and Table 4 lists the data for the blue survey list (30° Blue Survey; KB1). All three tables have precisely the same format; the contents are as follows: Column (1) gives the survey identification number (KISSR for the red surveys, KISSB for the blue survey). Table 5 correlates the KISSR and KISSB identification numbers for those objects included in both survey lists. Column (2) lists the survey field designation, and column (3) the field identification number. Column (4) identifies the observing run during which the spectrum was obtained (see Table 1). Column (5) gives a coarse spectral quality code: $Q = 1$ refers to high-quality spectra, with high signal-to-noise ratio (S/N) emission lines and reliable emission-line ratios. $Q = 2$ is assigned to spectra of lesser quality that still have reliable line ratios. $Q = 3$ refers to spectra where the data are of low quality, usually due to the faintness of the object and/or the weakness of the emission lines. (See Fig. 1 for examples). Column (6) gives the redshift of each object determined from the average of the redshifts derived from all strong emission lines. Typical formal uncertainties for z

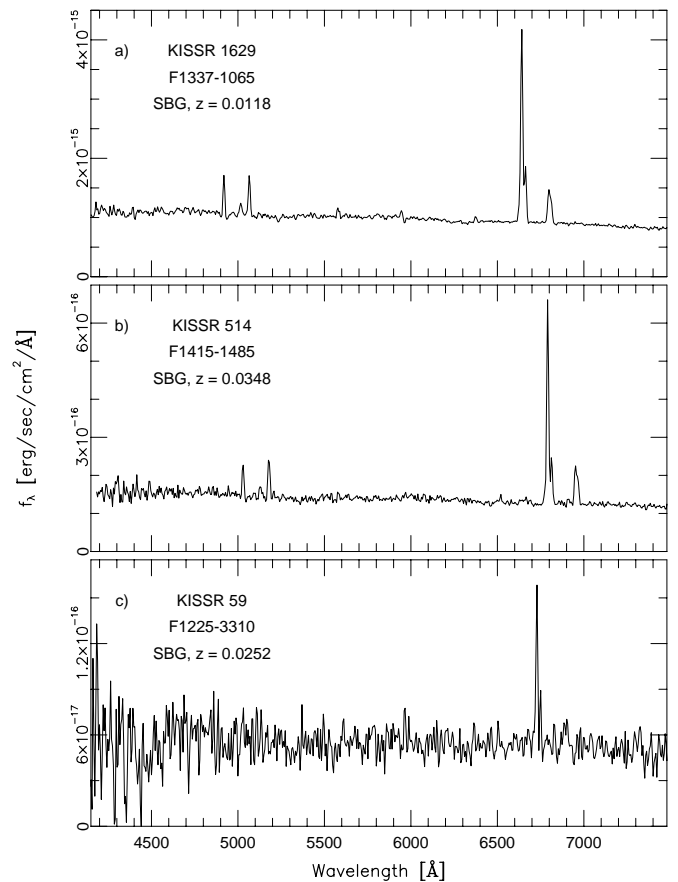


FIG. 1.—Sample MDM spectra of different spectral quality Q . (a) $Q = 1$, the line ratios $[O\text{ III}]/H\beta$, $[N\text{ II}]/H\alpha$, and $[S\text{ II}]/H\alpha$ can all be accurately determined, and $[He\text{ I}]\lambda 5876$ and $[O\text{ I}]\lambda 6300$ can be identified. (b) $Q = 2$, the S/N is lower, but the main line ratios are still reliable. (c) $Q = 3$, the line ratios that are measured have a lower degree of accuracy.

are 0.00010–0.00025 (30–75 km s⁻¹). Column (7) lists the decimal reddening coefficient $c_{H\beta}$. Columns (8) through (11) present the observed equivalent widths of $[O\text{ II}]\lambda\lambda 3726, 3729, H\beta, [O\text{ III}]\lambda 5007$, and $H\alpha$. The $H\alpha$ flux, in units of 10^{-16} ergs s⁻¹ cm⁻², is listed in column (12). These values should be treated with caution, since the observing conditions at MDM were not always photometric; see Table 1 for details. Columns (13) through (16) give the logarithms of the reddening-corrected line ratios ($[O\text{ II}]\lambda\lambda 3726, 3729/H\beta$), $[O\text{ III}]\lambda 5007/H\beta$, $[N\text{ II}]\lambda 6583/H\alpha$, and $[S\text{ II}]\lambda\lambda 6717, 6731/H\alpha$. If an equivalent width or line ratio measurement is not listed, either the relevant line was not present in the spectrum (often due to low S/N), or the line is redshifted out of the region covered by our spectra. For most of the objects observed at MDM, the $[O\text{ II}]$ doublet was not present in our observed spectral range. This is due to the lack of throughput of the spectrograph optics at wavelengths below 4000 Å. Finally, column (17) indicates the activity type for each object. The classifications of the ELGs are based primarily on the observed emission-line ratios (see Fig. 6), although factors like line widths are also used in the case of broad-lined objects (Seyfert 1 galaxies and QSOs). We identify seven classes: (SBG) starburst galaxy, (Sy1) Seyfert 1, (Sy2) Seyfert 2, (LIN) low ionization nuclear emission region (LINER), (QSO) quasi-stellar object, (Gal) non-emission-line galaxy, and (Star) Galactic star. The latter

TABLE 2
MDM SPECTROSCOPIC DATA: 30° RED SURVEY

KISSR (1)	FIELD (2)	ID (3)	RUN (4)	Q (5)	z (6)	α_{HB} (7)	EW (Å)					FLUX RATIOS ^b					TYPE (17)
							[O II] (8)	H β (9)	[O III] (10)	H α (11)	H α Flux ^a (12)	[O III]/H β (13)	[O III]/H β (14)	[N II]/H α (15)	[S II]/H α (16)		
11	F1215	1631	22	1	0.0752	0.94	...	15.39	8.49	89.20	272.756	...	-0.2616	-0.3430	-0.5484	SBG	
12	F1215	1627	22	1	0.0752	0.32	...	31.00	127.90	177.30	453.743	...	0.6122	-1.0961	-0.9595	SBG	
27	F1215	228	31	3	0.0031	3.26	198.326	-0.0437	-0.5407	LIN	
40	F1220	1974	31	1	0.0264	0.40	...	7.71	23.99	39.94	55.000	...	0.4830	-1.1102	-0.4400	SBG	
41	F1220	1793	32	2	0.0265	-0.02	...	5.26	...	13.08	39.460	-0.4591	-0.3614	SBG	
51	F1225	4904	152	3	0.0645	1.92	...	0.72	1.73	3.48	16.515	...	0.3518	-0.2123	-0.6306	LIN	
59	F1225	3310	31	3	0.0252	23.40	12.620 ^c	-0.5634	-0.4652	SBG	
60	F1225	2955	152	2	0.0581	1.35	...	5.89	5.45	20.43	84.854	...	-0.0852	-0.3600	-0.5518	SBG	
63	F1225	2549	31	2	0.0500	1.31	...	1.77	3.00	12.20	61.830	...	0.2438	-0.2092	-0.5139	LIN	
67	F1225	1225	153	1	0.0821	0.43	...	60.75	56.53	259.50	351.900	...	-0.0439	...	-1.5303	Sy1	
71	F1230	2940	31	2	0.0153	2.09	...	1.82	3.11	20.29	181.624 ^c	...	0.1954	-0.2697	-0.5260	LIN	
73	F1230	2407	151	2	0.0018	0.20	...	94.54	421.20	698.30	49.694	...	0.6229	-1.5308	-0.9456	SBG	
76	F1230	1857	32	1	0.0279	0.62	...	7.14	15.35	44.62	180.926	...	0.3346	-0.7258	-0.4859	SBG	
77	F1230	886	152	3	0.0623	1.04	...	2.08	...	6.09	18.211	-0.2897	-0.5114	SBG	
78	F1230	517	152	1	0.0511	0.77	...	11.51	1.89	19.57	157.507	...	-0.8318	-0.3313	-0.6487	SBG	
80	F1235	2775	32	2	0.0154	1.25	...	2.62	3.47	20.71	100.400	...	0.1070	-0.6340	-0.4218	SBG	
81	F1235	2737	153	3	0.0818	2.91	...	0.48	0.77	6.99	16.478	...	0.1149	-0.3039	-0.4726	SBG	
82	F1235	2583	152	3	0.0638	1.74	49.631	-0.1774	-0.5578	LIN	
84	F1235	1648	22	2	0.0578	0.95	...	4.30	4.68	24.00	196.556	...	0.0073	-0.4025	-0.4070	SBG	
112	F1245	4440	32	2	0.0231	1.15	...	1.03	2.32	6.94	69.608	...	0.3448	-0.1951	-0.1270	LIN	
113	F1245	4144	32	2	0.0231	0.61	...	9.56	6.96	48.49	125.600	...	-0.1024	-0.6367	-0.5355	SBG	
115	F1245	3820	32	1	0.0237	0.31	...	12.39	19.94	56.70	183.700	...	0.2189	-0.7719	-0.5658	SBG	
125	F1245	1285	32	2	0.0237	0.23	...	9.27	10.63	35.25	111.600	...	0.1071	-0.7700	-0.4818	SBG	
126	F1245	1219	32	2	0.0232	0.43	...	5.45	7.99	25.48	30.130	...	0.1826	-0.8922	-0.4992	SBG	
131	F1250	3617	153	2	0.0492	0.94	...	5.69	8.54	28.69	86.556	...	0.1464	-0.5763	-0.4748	SBG	
132	F1250	3207	31	2	0.0212	1.04	...	5.71	1.48	38.12	265.307 ^c	...	-0.6166	-0.3683	-0.5637	SBG	
136	F1250	1879	153	3	0.0330	9.45	37.660	-0.3956	-0.4606	SBG	
143	F1250	961	152	2	0.0268	1.59	...	3.22	1.51	15.80	67.550	...	-0.3759	-0.4562	-0.6279	SBG	
146	F1250	407	32	2	0.0078	0.07	...	24.89	18.35	49.82	23.210	...	0.1042	-0.6698	-0.5713	SBG	
147	F1250	355	31	3	0.0083	12.25	102.900 ^e	-0.4691	-0.5976	SBG	
148	F1250	317	32	1	0.0080	0.13	...	41.75	86.48	169.00	113.500	...	0.3779	-1.0258	-0.6405	SBG	
156	F1255	2049	32	2	0.0230	0.18	...	8.93	22.48	45.14	33.590	...	0.3646	-1.3005	-0.4676	SBG	
157	F1255	1719	31	2	0.0252	1.54	...	2.26	0.25	18.27	67.660 ^e	...	-0.9653	-0.4835	-0.6065	SBG	
164	F1255	557	153	3	0.0617	5.90	10.106	-0.3024	-0.3851	SBG	
172	F1300	2904	152	2	0.0844	Gal	
192	F1305	6848	21	2	0.0185	1.11	...	3.61	13.86	26.99	12.290	...	0.5568	-0.9505	-0.3116	SBG	
193	F1305	6506	21	2	0.0235	0.85	...	3.95	17.80	32.13	16.510	...	0.6229	-1.0190	-0.4646	SBG	
194	F1305	6633	22	1	0.0221	0.68	...	5.66	15.43	33.60	46.280	...	0.4178	-0.9415	-0.4320	SBG	
195	F1305	6062	22	3	0.0177	1.06	...	3.16	1.21	17.73	34.840	...	-0.3886	-0.5032	-0.5929	SBG	
196	F1305	5813	21	1	0.0267	0.29	...	137.90	575.60	853.00	585.481	...	0.5941	-1.2290	-0.8514	SBG	
197	F1305	5157	22	2	0.0236	0.04	...	9.48	4.10	30.39	62.830	...	-0.3036	-0.5754	-0.4239	SBG	
198	F1305	5095	22	3	0.0236	2.30	54.436	0.3023	0.1088	LIN	
199	F1305	4860	21	3	0.0236	5.04	16.14	12.290	-0.7707	-0.2294	SBG	
201	F1305	4760	22	3	0.0314	1.76	11.26	43.440	-0.3735	-0.4899	SBG	
202	F1305	4752	22	1	0.0161	0.40	...	11.82	27.50	62.22	231.200	...	0.3713	-0.9380	-0.5265	SBG	

TABLE 2—Continued

KISSR (1)	FIELD (2)	ID (3)	R _{UN} (4)	Q (5)	z (6)	c _{Hβ} (7)	EW (Å)				FLUX RATIOS ^b					TYPE (17)
							[O II] (8)	Hβ (9)	[O III] (10)	Hα (11)	Hα Flux ^a (12)	[O III]/Hβ (13)	[O III]/Hβ (14)	[N II]/Hα (15)	[S II]/Hα (16)	
203	F1305	4534	21	1	0.0615	...	12.46	16.54	65.70	214.892	...	0.1400	-0.5118	-0.5540	SBG
204	F1305	4183	22	3	0.0394	...	3.62	3.97	17.50	46.891	...	0.0516	-0.5146	-0.3504	SBG
205	F1305	3684	21	1	0.0175	...	11.16	44.92	59.66	85.100	...	0.6244	-1.2829	-0.7424	SBG
206	F1305	2976	21	2	0.0800	...	5.72	6.70	34.52	25.900	...	0.0333	-0.6160	-0.4590	SBG
207	F1305	2967	21	2	0.0247	...	2.97	9.03	47.89	24.280	...	0.4448	-1.2717	-0.4659	SBG
208	F1305	3013	22	3	0.0800	11.10	31.522	-0.4132	-0.3657	SBG
209	F1305	2884	22	3	0.0796	...	10.41	2.35	34.80	37.861	...	-0.5815	-0.4450	-0.4148	SBG
210	F1305	2697	21	3	0.0206	16.65	21.43	9.752	-0.7692	-0.3633	SBG
211	F1305	2635	22	2	0.0895	...	9.61	8.35	49.00	46.621	...	-0.0696	-0.4173	-0.5246	SBG
212	F1305	2217	21	1	0.0396	...	14.85	43.90	79.23	39.210	...	0.4511	-1.3506	-0.6260	SBG
213	F1305	2014	22	3	0.0393	...	28.27	31.61	30.12	4.793	...	0.2331	SBG
214	F1305	1987	21	1	0.0227	...	3.64	6.04	28.73	90.673	...	0.2043	SBG
215	F1305	1640	22	2	0.0228	...	3.48	...	24.55	64.250	-0.5261	-0.5364	SBG
216	F1305	1792	22	3	0.0317	13.02	23.100	-0.3957	-0.2758	SBG
217	F1305	1575	22	1	0.0187	...	10.41	11.76	54.80	62.215	...	0.0371	-0.7317	-0.4423	SBG
218	F1305	1126	21	1	0.0209	...	10.79	6.13	59.50	324.218	...	-0.2449	-0.3938	-0.4885	SBG
219	F1305	865	22	2	0.0791	...	4.56	4.10	32.00	57.390	...	-0.0440	-0.4316	-0.5095	SBG
220	F1305	943	22	1	0.0627	...	9.47	21.01	49.30	41.059	...	0.3367	-0.8304	-0.4227	SBG
221	F1305	381	22	2	0.0885	...	9.44	12.68	46.90	36.804	...	0.1379	-0.6128	-0.4306	SBG
222	F1305	354	21	1	0.0184	...	4.24	1.25	22.50	137.073	...	-0.5543	-0.2670	-0.5943	SBG
223	F1305	167	21	1	0.0842	...	44.49	222.90	208.70	72.583	...	0.7172	-1.1737	-0.9005	SBG
226	F1310	3423	31	3	0.0211	...	3.49	...	18.65	29.770 ^c	-0.4191	-0.9762	SBG
227	F1310	3267	31	3	0.0246	35.51	87.262 ^c	-0.2166	-0.5958	SBG
236	F1310	1263	32	3	0.0199	12.68	35.045	-0.3742	-0.2622	SBG
237	F1310	1010	152	3	0.0730	0.39	7.95	40.907	...	-0.8867	-0.3730	-0.8418	SBG
238	F1310	316	32	3	0.0218	...	1.29	5.96	13.16	29.930	...	0.6221	-0.5530	-0.5478	SBG
241	F1315	4343	32	1	0.0227	...	8.63	4.39	61.63	288.900	...	-0.3242	-0.4568	-0.5636	SBG
245	F1315	3173	32	1	0.0159	...	6.73	16.22	36.15	91.000	...	0.3844	-0.8289	-0.4757	SBG
258	F1315	1234	22	1	0.0754	...	27.12	76.93	128.80	80.037	...	0.4495	-0.7087	-0.5334	SBG
269	F1320	3988	153	2	0.0486	...	4.00	2.42	20.20	69.187	...	-0.2639	-0.4298	-0.6189	SBG
270	F1320	3806	32	2	0.0231	...	4.67	...	13.75	25.670	-0.4456	-0.3415	SBG
271	F1320	3150	32	1	0.0226	...	5.64	13.18	28.73	73.420	...	0.3950	-1.0158	-0.4466	SBG
278	F1320	1206	32	1	0.0135	...	14.37	47.26	61.70	55.270	...	0.5254	-1.3319	-0.6665	SBG
280	F1320	704	32	1	0.0183	...	13.55	33.41	49.88	58.710	...	0.4371	-1.2755	-0.6505	SBG
281	F1320	262	23	1	0.0726	...	23.29	15.44	152.90	337.518 ^c	...	-0.2325	Sy1
282	F1320	226	31	1	0.0233	...	3.00	42.59	16.54	54.050	...	1.1382	0.0104	-0.2473	Sy2
286	F1325	3189	23	1	0.0172	...	61.63	281.90	296.00	1021.117 ^c	...	0.6411	-1.2712	-0.8685	SBG
291	F1325	1117	153	3	0.0365	...	1.20	...	11.60	51.002	-0.4180	-0.6412	SBG
295	F1325	652	152	2	0.0758	...	4.00	2.02	9.40	92.791	...	-0.3327	-0.3407	-0.5736	SBG
299	F1330	5795	23	1	0.0262	...	15.40	48.42	71.14	144.647 ^c	...	0.5151	-1.0864	-0.5456	SBG
300	F1330	5190	31	3	0.0247	...	4.11	7.93	19.08	13.510	...	0.3126	-0.8310	-0.4759	SBG
314	F1335	3744	31	1	0.0029	...	6.47	19.00	35.11	128.000 ^c	...	0.4801	-1.2845	-0.5970	SBG
316	F1335	3422	153	3	0.0389	...	1.06	0.30	6.11	25.395	-0.4008	-0.4577	SBG
320	F1335	2158	31	2	0.0266	...	3.30	2.46	20.17	32.732	...	-0.1273	-0.4837	-0.3004	SBG
323	F1335	1106	151	3	0.0436	...	3.68	23.50	48.75	20.018	...	0.7110	-1.0738	-0.5856	SBG
324	F1335	806	152	3	0.0327	...	1.47	...	5.97	36.091	-0.3717	-0.6977	SBG

TABLE 2—Continued

KISSR (1)	FIELD (2)	ID (3)	R _{UN} (4)	Q (5)	z (6)	c _{Hβ} (7)	EW (Å)				FLUX RATIOS ^b						TYPE (17)
							[O II] (8)	Hβ (9)	[O III] (10)	Hα (11)	Hα Flux ^a (12)	[O II]/Hβ (13)	[O III]/Hβ (14)	[N II]/Hα (15)	[S II]/Hα (16)		
332	F1340	4534	151	3	0.0448	2.29	...	0.63	1.16	3.47	27.482	...	0.2040	-0.1977	-0.4335	LIN	
344	F1340	1751	153	3	0.0345	4.90	15.798	-0.3759	-0.4148	SBG	
348	F1345	4123	152	1	0.0398	0.96	...	9.89	17.42	28.26	133.994	...	0.1971	-0.6103	-0.5517	SBG	
350	F1345	3363	22	1	0.0766	0.71	...	28.76	20.35	181.50	1118.000	...	-0.1811	...	-1.3903	Sy1	
353	F1345	1382	151	3	0.0632	2.01	27.616	-0.3686	-0.5250	LIN	
374	F1350	2887	152	2	0.0357	0.89	...	11.57	3.04	25.66	122.666	...	-0.6250	-0.4588	SBG		
386	F1350	414	32	1	0.0240	0.39	...	7.51	18.42	35.54	62.460	...	0.3914	-0.8918	SBG		
394	F1355	5189	153	3	0.0349	9.26	17.603	-0.4144	-0.4274	SBG	
396	F1355	4898	23	1	0.0077	-0.02	...	48.76	212.90	226.30	592.871 ^c	...	0.6362	-1.5771	-0.9326	SBG	
399	F1355	4788	152	1	0.0375	0.60	...	22.58	19.79	26.96	268.756	...	-0.0971	-0.6286	-0.5779	SBG	
401	F1355	4736	151	1	0.0369	0.24	...	94.69	276.50	124.70	79.889	...	0.3464	-0.8895	-0.7210	SBG	
406	F1355	2803	153	3	0.0386	3.43	0.68	14.163	0.1582	0.0502	LIN	
408	F1355	2588	31	3	0.0191	3.20	8.66	15.450	-0.6781	-0.1967	SBG	
407	F1355	2689	153	3	0.0390	1.24	14.992	-0.1415	-0.1724	LIN	
410	F1355	1934	22	1	0.0771	0.63	...	18.73	18.20	116.30	210.566	...	-0.0607	-0.5082	-0.3371	SBG	
419	F1400	4930	32	1	0.0605	1.06	...	6.60	14.94	39.47	246.468	...	0.3281	-0.1978	-0.5304	LIN	
421	F1400	4177	23	1	0.0274	0.44	...	32.12	47.23	147.50	783.691 ^c	...	0.1748	-0.6807	-0.7941	SBG	
422	F1400	4082	32	2	0.0263	1.76	...	1.94	1.34	17.99	164.656	...	-0.1998	-0.1631	-0.4391	SBG	
428	F1400	2666	22	2	0.0637	1.26	...	6.14	3.47	50.90	173.731	...	-0.2691	-0.4407	-0.6314	SBG	
429	F1400	2267	32	2	0.0728	1.20	...	6.49	2.39	45.80	198.405	...	-0.4549	-0.3711	-0.7160	SBG	
433	F1400	1190	32	2	0.0636	1.68	...	1.34	0.98	15.26	121.754	...	-0.3094	-0.3175	-0.4300	SBG	
439	F1400	616	23	3	0.0778	1.28	...	3.70	0.88	25.90	230.376 ^c	...	-0.6160	-0.4409	-0.6931	SBG	
466	F1405	96	32	3	0.0643	12.01	27.362	-0.1546	-0.5376	LIN	
470	F1410	5809	31	2	0.0218	0.78	...	4.22	...	24.09	45.340	-0.5017	-0.4683	SBG	
497	F1415	5070	23	1	0.0856	1.07	...	4.09	19.02	23.10	108.864 ^c	...	0.6422	-0.1055	-0.2063	Sy2	
505	F1415	3598	23	1	0.0110	0.54	...	6.07	26.12	38.23	154.333 ^c	...	0.6194	-1.3919	-0.6052	SBG	
509	F1415	3127	23	1	0.0354	0.44	...	22.92	38.62	130.80	265.202 ^c	...	0.1847	-0.7240	-0.5206	SBG	
510	F1415	3114	23	2	0.0351	1.65	...	3.72	2.59	28.60	268.551 ^c	...	-0.1676	-0.2821	-0.5785	SBG	
511	F1415	2703	23	3	0.0770	3.30	...	0.50	1.32	16.20	130.602 ^c	...	0.3347	-0.3130	-0.6656	SBG	
512	F1415	2664	23	2	0.0778	0.41	...	32.66	11.99	83.40	134.739 ^c	...	-0.3159	-0.3636	-0.3953	SBG	
513	F1415	2486	152	3	0.0352	4.61	13.702	-0.3608	-0.4603	SBG	
514	F1415	1485	153	2	0.0348	1.11	29.13	70.960	...	0.1139	-0.6722	-0.5248	SBG	
526	F1420	4974	32	3	Star	
526	F1420	4474	23	1	0.0884	1.13	Star	
533	F1420	2709	153	2	0.0546	92.30	446.042 ^c	...	-0.3613	-0.4138	-0.6358	SBG	
541	F1420	1035	31	3	0.0102	1.45	5.74	Gal	
544	F1420	701	31	2	0.0297	0.53	...	1.44	15.37	14.93	25.390	...	0.5669	-0.7586	-0.3959	SBG	
550	F1425	3837	153	3	0.0393	7.45	...	36.51	35.790	...	0.3168	-0.8410	-0.3598	SBG	
552	F1425	2180	152	3	0.0300	1.16	16.158	-0.0354	-0.4165	LIN	
559	F1425	359	31	2	0.1165	0.05	9.60	22.660	-0.3293	-0.3949	SBG	
561	F1425	46	31	1	0.0121	-0.15	...	21.91	...	61.96	21.323	-0.6446	-0.4239	Gal	
562	F1445	6832	153	2	0.0770	1.41	...	34.97	69.38	100.20	28.340	...	0.4749	-1.2391	-0.7104	SBG	
564	F1445	6520	112	2	0.0326	0.67	...	3.33	3.52	18.32	61.241	...	-0.0230	-0.4615	-0.5075	SBG	
565	F1445	6313	31	3	5.53	17.06	12.71	36.435 ^c	...	0.4963	-0.7979	-0.4095	SBG	
572	F1445	4508	23	1	0.0124	-0.08	Star	
575	F1445	2895	152	3	0.0457	1.27	...	12.87	18.79	39.73	73.028 ^c	...	0.2295	-1.0865	-0.5158	SBG	
							...	3.64	3.02	13.75	52.608	...	-0.1259	-0.4088	-0.5137	SBG	

TABLE 2—Continued

KISSR (1)	FIELD (2)	ID (3)	R _{UN} (4)	Q (5)	z (6)	c _{Hβ} (7)	EW (Å)				FLUX RATIOS ^b					TYPE (17)
							[O II] (8)	Hβ (9)	[O III] (10)	Hα (11)	Hα Flux ^a (12)	[O III]/Hβ (13)	[O III]/Hβ (14)	[N II]/Hα (15)	[S II]/Hα (16)	
584	F1450	3971	153	2	0.0589	1.29	...	31.46	2.26	40.941	...	1.2016	-0.0174	-0.1786	Sy2	
586	F1450	925	31	3	0.0228	9.47	141.516	-0.1922	-0.3872	Sy2	
589	F1450	588	23	2	0.0227	1.08	...	7.75	26.90	69.493 ^c	...	0.3411	-0.7337	-0.4915	SBG	
590	F1455	8836	23	1	0.0309	0.21	...	63.21	100.50	95.515 ^e	...	0.3780	-0.8639	-0.4703	SBG	
592	F1455	7974	32	2	0.0564	1.07	...	5.95	49.75	107.859	...	-0.1765	-0.3760	-0.4442	SBG	
596	F1455	6890	152	3	0.0783	2.35	16.555	-0.0472	-0.2453	LIN	
603	F1455	774	32	1	0.3420	0.74	21.28	98.00	34.87	17.360	0.7267	1.3844	0.0414	...	Sy2	
618	F1500	4372	22	1	0.0722	2.16	...	8.81	15.10	58.749	...	0.8536	-0.1924	-0.6151	Sy2	
620	F1500	3934	153	3	0.0821	1.76	...	2.39	10.70	16.245	...	0.0701	-0.3756	-0.4179	SBG	
621	F1500	3752	152	1	0.0715	0.74	...	15.22	31.12	113.569	...	0.0415	-0.5880	-0.5085	SBG	
627	F1505	4937	152	3	0.0806	5.41	34.184	-0.2419	-0.6366	SBG	
629	F1505	4792	153	3	0.0817	0.96	...	0.53	5.74	11.195	...	-0.3791	-0.3735	-0.2437	SBG	
648	F1510	5453	32	3	Star	
651	F1510	4905	153	3	0.0584	1.34	...	1.28	7.05	41.599	...	-0.3215	-0.3323	-0.5913	SBG	
653	F1510	4675	152	1	0.0697	0.43	...	51.33	74.33	230.270	...	0.2298	-0.7771	-0.6423	SBG	
665	F1515	5655	153	1	0.0871	0.33	...	212.90	117.00	101.007	...	0.5929	-1.1721	-0.7359	SBG	
666	F1515	5729	32	1	0.0332	0.11	...	890.10	807.90	107.300	...	0.8110	-2.0621	-1.4086	SBG	
669	F1515	4627	32	2	0.0313	1.80	...	2.08	22.84	102.877	...	-0.6990	-0.3796	-0.7164	SBG	
678	F1515	2600	32	1	0.0330	0.67	...	10.21	57.48	56.950	...	0.2806	-0.7760	-0.5063	SBG	
688	F1520	6259	23	1	0.0773	0.90	...	191.70	172.60	44.812 ^c	...	0.6730	-1.0866	...	SBG	
690	F1520	5577	23	3	0.0753	1.13	...	3.76	33.20	61.529 ^c	...	-0.0646	-0.4790	-0.4778	SBG	
693	F1520	4216	23	3	0.0758	0.53	...	4.16	15.50	37.431 ^c	-0.3604	-0.3259	SBG	
696	F1520	4121	23	2	0.0756	0.28	...	25.44	52.68	44.520 ^c	...	0.3160	-0.9068	-0.4615	SBG	
700	F1520	3904	23	1	0.0728	0.41	...	31.13	8.40	34.522 ^c	...	1.1261	-0.0470	-0.2632	Sy2	
707	F1520	2625	23	2	0.0229	1.17	...	0.97	35.80	361.210 ^c	...	-0.7389	-0.4223	-0.7001	SBG	
708	F1520	2623	23	3	0.0779	7.60	20.307 ^c	LIN	
717	F1520	1404	23	1	0.0869	1.26	...	134.80	78.10	373.921 ^c	...	1.1003	-0.0016	-0.2511	Sy2	
725	F1525	7575	23	1	0.0314	0.30	...	14.26	41.55	67.248 ^c	...	0.1816	-0.7515	...	SBG	
738	F1525	5541	152	3	0.0752	2.35	...	4.51	3.85	37.787	...	0.8028	-0.2895	-0.7041	Sy2	
747	F1525	4370	152	2	0.0563	0.85	...	7.68	25.10	73.831	...	-0.0340	-0.5050	-0.5258	SBG	
748	F1525	4493	152	3	0.0669	1.37	...	1.07	4.49	16.034	...	-0.3052	-0.4344	-0.5441	SBG	
749	F1525	4291	153	3	0.0751	6.93	13.860	-0.3496	-0.4033	SBG	
751	F1525	4260	153	2	0.0345	1.94	...	0.45	10.38	79.018	...	-0.6108	-0.4000	-0.7181	SBG	
758	F1525	2618	152	3	0.0817	1.97	...	2.65	13.75	45.543	...	-0.0305	-0.4880	-0.5568	SBG	
809	F1530	273	32	3	0.0369	4.24	19.38	12.450	-0.7703	-0.4756	SBG	
826	F1535	3155	153	2	0.0605	1.04	...	6.28	18.36	124.541	-0.1576	-0.4968	SBG	
833	F1535	1253	31	1	0.0602	0.71	...	14.13	86.55	322.186	...	-0.1212	-0.5165	-0.4932	SBG	
838	F1540	5141	32	2	0.3511	...	58.23	203.30	...	24.707	Sy2	
839	F1540	4914	31	1	0.0820	0.93	...	94.41	35.16	24.707	...	1.1708	-0.1772	-0.3060	Sy2	
842	F1540	3988	153	2	Star	
844	F1540	2359	31	1	0.4558	0.35	13.03	162.00	-0.7642	0.0519	QSO	
846	F1540	1216	112	2	0.0589	1.45	...	1.58	6.88	86.093 ^c	...	-0.3750	-0.4014	-0.5312	SBG	
847	F1540	805	23	1	0.3558	1731.00	Sy2	
848	F1540	275	152	2	0.0830	0.71	...	5.68	34.81	81.537	...	-0.4176	-0.5165	-0.5910	SBG	
853	F1545	5825	31	2	0.0310	1.18	...	3.87	20.96	74.745	...	0.1692	-0.5094	-0.3669	SBG	
871	F1550	9263	152	3	0.0734	7.99	16.657	-0.4008	-0.4657	SBG	

TABLE 2—Continued

KISSR (1)	FIELD (2)	ID (3)	R _{UN} (4)	Q (5)	z (6)	c _{Hβ} (7)	EW (Å)				FLUX RATIOS ^b					TYPE (17)
							[O II] (8)	Hβ (9)	[O III] (10)	Hα (11)	Hα Flux ^a (12)	[O II]/Hβ (13)	[O III]/Hβ (14)	[N II]/Hα (15)	[S II]/Hα (16)	
875	F1550	8714	31	3	0.0753	19.11	31.699	-0.2940	-0.3241	SBG
876	F1550	8206	151	2	0.0626	1.12	0.62	9.96	51.925	-0.7306	-0.3037	-0.6246	SBG
880	F1550	5584	151	2	0.0780	2.06	1.48	13.84	30.255	-0.1620	-0.5055	-0.5024	SBG
883	F1550	4243	31	3	Star
891	F1550	2635	32	1	0.0338	0.13	26.17	44.89	46.630	0.4044	-0.9788	-0.5479	SBG
913	F1555	8067	23	1	0.0310	0.85	23.16	56.38	115.696 ^c	0.4545	-0.9323	-0.4433	SBG
924	F1555	6214	22	1	0.0855	0.76	7.50	289.30	2700.000	-0.8116	Sy1
933	F1555	4565	153	2	0.0700	0.84	1.69	14.37	41.153	-0.5111	-0.3784	-0.5227	SBG
937	F1555	2356	31	3	0.0783	1.13	...	22.04	28.945	-0.2304	-0.3126	SBG
939	F1555	2186	152	2	0.0770	1.34	0.72	17.96	61.365	-0.7304	-0.4327	-0.7103	SBG
947	F1600	6052	112	3	0.0770	3.12	1.57	5.38	14.530 ^c	0.5003	-0.3141	-0.3987	SBG
953	F1600	4716	152	3	0.0774	1.71	4.03	10.28	40.610	0.1875	-0.3422	-0.4914	SBG
955	F1600	3730	32	1	0.0319	0.41	84.27	117.90	169.800	0.6206	-1.4019	-0.7023	SBG
956	F1600	3594	31	1	0.0143	0.69	18.93	32.57	44.050	0.5029	-0.8780	-0.4367	SBG
962	F1605	9133	32	3	Gal
964	F1605	7625	23	1	0.0311	0.51	21.32	85.75	346.589 ^c	0.1200	-0.7543	-0.5006	SBG
970	F1605	5334	153	3	0.0882	1.63	0.94	15.70	36.486	-0.4857	-0.4791	-0.6692	SBG
971	F1605	5356	31	1	0.3282	0.09	67.82	207.58	133.500	-0.4790	...	0.2245	Sy1
972	F1605	4640	153	2	0.0916	1.34	1.16	11.14	52.527	-0.5766	-0.3220	-0.5119	SBG
976	F1605	2721	153	2	0.0866	1.00	5.52	16.77	17.500	0.1511	-0.5587	-0.4582	SBG
979	F1605	1899	151	1	0.0329	0.21	72.03	55.03	43.779	0.5497	-1.1521	-0.6141	SBG
980	F1605	1786	31	3	Star
981	F1605	1806	31	1	0.0231	0.70	5.84	28.64	42.340	0.0640	-0.7440	-0.4091	SBG
985	F1610	7809	21	1	0.0419	0.55	47.17	96.20	95.843	0.4126	-0.8314	-0.6478	SBG
986	F1610	7502	22	1	0.0672	-0.10	211.00	202.20	28.380	0.6187	-2.2019	-0.9477	SBG
987	F1610	7225	21	1	0.0415	0.85	9.44	32.31	40.190	0.2773	-0.8916	-0.4195	SBG
988	F1610	6757	21	3	0.0876	3.37	0.75	26.70	52.970	-0.2497	-0.6970	SBG
989	F1610	5617	22	2	0.0334	1.16	6.79	21.70	41.767	0.3810	-0.5945	-0.3324	SBG
990	F1610	5386	21	3	0.0522	1.03	2.07	13.40	23.531	-0.3454	-0.4395	SBG
991	F1610	5038	22	1	0.0914	1.09	1.36	44.10	63.636	-0.7755	-0.4203	-0.6760	SBG
992	F1610	4551	21	2	0.0504	1.07	...	25.40	51.360	-0.4601	-0.7387	SBG
993	F1610	4718	21	3	0.0878	1.12	2.45	12.60	11.486	-0.0041	-0.3235	-0.4003	SBG
994	F1610	4617	22	3	0.0345	10.90	34.813	-0.3362	-0.4318	SBG
995	F1610	4473	22	1	0.0528	0.25	56.15	78.34	25.220	0.5519	-1.1858	-0.6294	SBG
996	F1610	4073	22	3	0.0533	1.24	2.65	15.10	45.708	0.0485	-0.2960	-0.4657	SBG
997	F1610	3900	23	1	0.0539	0.98	9.54	5.90	60.119 ^c	0.9017	0.2636	-0.0135	Sy2
998	F1610	3862	22	1	0.0340	0.80	...	81.00	57.271	-0.6198	-0.8395	SBG
999	F1610	3713	21	3	0.0325	7.16	16.960	-0.4562	-0.5500	SBG
1000	F1610	3054	21	2	0.0622	1.01	...	36.80	20.919	-0.4363	-0.3402	SBG
1001	F1610	2746	21	2	Star
1002	F1610	2644	21	1	0.0612	1.25	7.97	27.30	61.506	0.2865	-0.2416	-0.5566	LIN
1003	F1610	2475	21	3	0.0805	0.82	4.72	35.00	25.586	-0.1316	-0.5119	-0.5287	SBG
1004	F1610	1418	21	2	0.0308	1.28	5.09	2.67	9.273	0.9968	0.3615	-0.0972	Sy2
1005	F1610	895	22	3	0.0338	-0.02	3.21	21.60	12.070	-0.3137	-0.7977	-0.2391	SBG
1006	F1610	829	21	3	0.0852	0.85	9.75	55.23	11.080	0.0684	-0.6571	-0.4366	SBG
1007	F1610	585	21	1	0.0342	0.69	3.66	53.60	250.827	-0.4001	-0.2932	-0.6536	SBG

TABLE 2—Continued

KISSR (1)	FIELD (2)	ID (3)	RUN (4)	Q (5)	z (6)	$\zeta_{H\beta}$ (7)	EW (Å)				FLUX RATIOS ^b							TYPE (17)
							[O II] (8)	H β (9)	[O III] (10)	H α (11)	H α FLUX ^a (12)	[O III]/H β (13)	[O III]/H β (14)	[N II]/H α (15)	[S II]/H α (16)			
1008	F1610	22	3	0.0789	-0.11	2.68	...	5.77	16.410	-0.7947	...	SBG			
1011	F1615	31	3	0.0081	3.48	5.39	9.417	-1.0427	-0.1754	SBG			
1013	F1615	23	2	0.0249	-0.07	32.22	82.14	95.33	51.569 ^c	...	0.4453	-1.8206	...	SBG			
1014	F1615	151	1	0.0330	0.34	33.50	111.30	108.40	61.740	...	0.5253	-1.1620	-0.7902	SBG			
1021	F1615	23	2	0.0086	0.31	12.89	44.27	67.93	77.374 ^c	...	0.4774	-1.7842	-0.6624	SBG			
1022	F1615	153	3	0.0835	1.80	1.42	...	7.46	21.952	-0.4185	-0.7431	SBG			
1025	F1620	6141	1	0.0869	0.82	8.17	14.06	33.53	53.065	...	0.2073	-0.6799	-0.5453	SBG			
1048	F1630	1486	32	1	0.0031	72.76	131.50	329.00	256.300	...	0.3145	-1.0568	-0.6346	SBG			
1061	F1635	1779	31	2	0.0870	2.42	...	20.05	47.650	-0.2845	-0.6440	SBG			
1063	F1640	9350	31	2	0.1016	6.32	4.15	42.39	51.750	...	-0.2045	-0.4605	-0.5838	Gal			
1066	F1640	8093	31	3	Star			
1074	F1645	9650	22	1	Star			
1078	F1645	4973	31	1	0.0533	7.90	3.29	53.93	188.200	...	-0.3782	-0.5147	-0.5770	SBG			
1080	F1645	2617	32	2	0.0363	5.86	1.10	22.82	64.036	...	-0.6990	-0.3730	-0.4062	SBG			
1084	F1645	769	31	1	0.0321	15.29	11.92	83.77	408.075	...	-0.1171	-0.3632	-0.6077	SBG			
1086	F1645	776	152	3	0.0784	5.37	16.329	-0.2685	-0.5034	SBG			
1089	F1650	10969	153	2	0.0786	7.39	3.92	30.99	53.669	...	-0.2931	-0.4868	-0.5073	SBG			
1094	F1650	8621	31	1	0.0327	19.37	31.62	113.20	629.200	...	0.2095	-0.7570	-0.7223	SBG			
1109	F1650	583	153	2	0.0709	5.56	4.67	20.75	93.473	...	-0.1278	-0.4489	-0.5052	SBG			
1111	F1655	11037	152	1	0.0727	8.86	16.32	41.86	118.789	...	0.2319	-0.6156	-0.5240	SBG			
1112	F1655	8821	32	3	0.0358	7.03	8.52	21.07	4.908	...	0.1460	...	-0.3447	SBG			
1127	F1655	605	32	1	0.0321	9.41	4.63	52.83	245.570	...	-0.3152	-0.4723	-0.5009	SBG			

^a In units of 10^{-16} ergs s^{-1} cm^{-2} .

^b In logarithmic units.

^c Observation made under nonphotometric conditions.

TABLE 3
MDM SPECTROSCOPIC DATA: 43° RED SURVEY

KISSR (1)	FIELD (2)	ID (3)	RUN (4)	Q (5)	z (6)	c _{Hβ} (7)	EW (Å)				FLUX RATIOS ^b					TYPE (17)
							[O III] (8)	Hβ (9)	[O III] (10)	Hα (11)	Hα FLUX ^a (12)	[O III]/Hβ (13)	[O III]/Hβ (14)	[N III]/Hα (15)	[S III]/Hα (16)	
1136	F1155	4700	111	3	0.0674	1.41	1.83	...	19.08	84.558	-0.4132	-0.5667	SBG	
1138	F1155	4513	112	2	0.0233	1.69	1.06	27.33	3.83	96.360	...	1.3593	-0.1720	-0.2517	Sy2	
1140	F1155	4556	111	3	0.0666	7.67	41.696	-0.0959	-0.2836	LIN	
1146	F1155	3081	112	3	0.0237	7.93	241.387	-0.4095	-0.6965	SBG	
1147	F1155	3518	112	1	0.0879	0.95	3.81	51.87	1.46	81.470	...	1.0763	0.0466	-0.1776	Sy2	
1149	F1155	3531	151	2	0.0735	2.78	0.48	13.01	3.09	45.379 ^c	...	1.3547	-0.0807	-0.5578	Sy2	
1150	F1155	3044	112	1	0.0363	0.94	8.20	4.38	21.00	179.263	...	-0.3122	-0.4830	-0.5552	SBG	
1155	F1155	1282	112	2	0.0252	1.23	3.01	5.66	6.20	190.608	...	0.2573	-0.2150	-0.5135	LIN	
1158	F1155	1803	112	2	0.0696	1.34	4.34	1.13	11.42	129.953	...	-0.6171	-0.4505	-0.6331	SBG	
1165	F1200	5692	111	2	0.0700	1.14	2.59	...	21.47	99.575	-0.3819	-0.7301	SBG	
1171	F1200	5712	112	1	0.0317	1.33	6.31	56.45	0.99	645.991	...	0.9052	0.0033	-0.3869	Sy2	
1207	F1204	2114	112	2	0.0548	1.86	1.00	17.93	12.00	14.410	...	1.1621	0.2765	-0.3725	Sy2	
1224	F1208	1631	112	1	0.0379	0.89	4.56	90.88	0.87	126.290	...	1.2677	0.0623	-0.3486	Sy2	
1226	F1208	2040	112	1	0.3094	1.95	7.42	205.30	138.40	78.620	0.9508	1.2726	Sy1	
1241	F1212	2133	111	1	0.0748	1.40	5.64	21.83	59.58	141.961	...	0.5683	-0.1268	-0.6392	Sy2	
1262	F1217	3746	111	3	0.0658	2.14	1.09	0.52	19.82	136.606	...	-0.3821	-0.3426	-0.5929	SBG	
1274	F1217	1590	111	1	0.0244	0.75	9.93	2.23	85.64	946.959	...	-0.6811	-0.3355	-0.7559	SBG	
1276	F1217	1573	112	3	0.0667	2.43	1.58	...	4.78	27.115	-0.2548	-0.3587	SBG	
1302	F1225	1177	111	2	0.0863	1.35	5.32	7.12	53.25	68.503	...	0.1026	-0.4146	-0.4956	Sy2	
1304	F1225	12	112	1	0.3478	1.19	5.67	163.90	91.18	13.820	0.7833	1.3899	Sy2	
1363	F1242	4496	111	2	0.0735	1.02	5.86	...	39.98	56.686	-0.2349	-0.7473	SBG	
1382	F1251	5361	111	1	0.0624	0.55	33.78	122.60	270.70	1000.575	...	0.5215	-0.3879	-0.7019	Sy2	
1406	F1259	3725	112	3	0.0579	2.66	0.60	...	3.67	70.349	-0.3474	-0.8140	SBG	
1412	F1259	2360	111	1	0.0590	1.59	10.04	14.69	134.10	87.508	...	0.1144	0.2541	-0.0993	Sy2	
1415	F1259	470	111	1	0.0535	0.40	36.36	122.10	224.60	558.174	...	0.4829	-0.9192	-0.6700	SBG	
1439	F1303	790	112	3	0.0274	1.62	6.30	53.709	-0.4045	-0.3661	SBG	
1441	F1303	290	111	2	0.0394	1.85	2.27	3.06	20.36	60.369	...	0.1217	0.0147	-0.4024	LIN	
1461	F1308	3356	111	3	0.0358	3.20	3.23	49.131	0.2789	0.1499	LIN	
1487	F1312	3083	112	1	0.0616	1.12	7.60	3.95	15.49	333.407	...	-0.3051	-0.4253	-0.6083	SBG	
1494	F1312	2201	112	1	0.0573	1.21	5.97	24.60	3.79	316.071	...	0.5810	-0.1546	-0.5254	Sy2	
1511	F1316	6831	112	2	0.0861	0.45	31.64	9.49	150.60	435.600	...	-0.5381	Sy1	
1527	F1316	2389	112	2	0.0280	0.89	3.03	0.71	5.25	152.743	...	-0.6520	-0.3006	-0.5834	SBG	
1530	F1316	1065	112	1	0.0761	1.48	6.07	5.48	11.33	133.930	...	-0.0862	-0.4205	-0.5058	SBG	
1554	F1320	1357	111	1	0.0744	1.00	5.81	17.12	50.26	153.530	...	0.4323	-0.2716	-0.4916	LIN	
1556	F1325	6483	111	1	0.0275	1.42	4.12	47.70	41.62	355.681	...	1.0311	0.0263	-0.4283	Sy2	
1568	F1325	4279	112	2	0.0042	1.78	2.78	0.26	9.46	656.745	...	-1.0597	-0.3850	-0.6866	SBG	
1578	F1329	4742	111	1	0.0279	0.16	76.47	330.70	441.90	1655.086	...	0.6124	-1.1774	-0.8681	SBG	
1589	F1329	1898	112	1	0.0274	0.71	13.85	5.71	18.46	398.616	...	-0.4098	-0.4029	-0.5865	SBG	
1592	F1333	5857	112	3	0.0336	1.27	3.04	1.54	6.19	60.685	...	-0.3059	-0.3444	-0.3790	SBG	
1600	F1333	3226	151	2	0.3741	...	26.82	426.80	Sy2	
1629	F1337	1065	111	1	0.0118	0.87	8.08	9.19	56.81	461.657	...	0.0324	-0.5445	-0.5746	SBG	
1631	F1337	471	112	2	0.0625	1.15	6.98	4.46	10.33	119.694	...	-0.2024	-0.4086	-0.5193	SBG	
1633	F1342	4841	112	2	0.0523	1.19	5.67	1.61	8.46	163.272	...	-0.5612	-0.4071	-0.5822	SBG	
1683	F1359	2988	111	2	0.0726	1.50	3.39	1.83	42.07	99.433	...	-0.3076	-0.6107	-0.3534	SBG	
1691	F1359	426	111	3	0.0323	2.62	1.09	0.54	19.30	69.532	...	-0.3418	-0.2553	-0.5500	SBG	

TABLE 3—Continued

KISSR (1)	FIELD (2)	ID (3)	R _{UN} (4)	Q (5)	z (6)	c _{Hβ} (7)	EW (Å)				FLUX RATIOS ^b					TYPE (17)
							[O III] (8)	Hβ (9)	[O III] (10)	Hα (11)	Hα FLUX ^a (12)	[O III]/Hβ (13)	[O III]/Hβ (14)	[N III]/Hα (15)	[S III]/Hα (16)	
1692	F1359	111	1	0.0331	2.07	...	6.59	2.07	80.83	278.626	...	-0.5448	-0.2814	-0.6237	SBG
1743	F1411	111	2	0.0862	1.20	...	4.09	3.62	40.02	64.416	...	-0.0946	-0.4355	-0.6400	SBG
1747	F1416	112	1	0.0693	0.73	...	15.13	6.04	13.23	173.052	...	-0.3986	-0.3613	-0.5951	SBG
1764	F1420	111	3	0.0763	3.82	4.56	67.602	-0.2939	...	SBG
1811	F1433	111	2	0.0877	2.02	...	2.69	1.69	51.26	68.625	...	-0.2625	-0.2744	-0.6353	SBG
1844	F1441	151	3	0.0362	1.97	...	1.76	...	16.91	34.027	-0.4124	-0.5986	SBG
1857	F1445	112	2	0.0438	1.44	...	5.21	0.77	10.36	172.049	...	-0.8711	-0.4494	-0.6918	SBG
1869	F1450	111	2	0.0182	1.83	...	1.93	5.59	28.36	164.433	...	0.4179	-0.5326	-0.5076	SBG
1895	F1502	111	2	0.0420	1.36	...	4.78	...	39.75	130.318	-0.1519	-0.5838	SBG
1919	F1511	112	3	0.0655	1.70	...	2.12	1.30	3.95	87.062	...	-0.2454	-0.2385	-0.6612	SBG
1930	F1515	112	2	0.0180	2.45	...	0.89	2.46	14.36	117.837	...	0.4168	0.0074	0.0344	LIN
1961	F1532	112	3	0.0528	2.12	...	2.78	2.44	4.63	54.052	...	-0.0978	-0.2032	-0.5067	SBG
1971	F1532	111	1	0.0726	1.29	...	7.04	14.81	67.94	154.146	...	0.2833	-0.6286	-0.4695	SBG
1976	F1532	112	3	0.0618	1.70	...	3.12	4.78	7.49	34.468 ^c	...	0.2071	-0.4585	-0.5349	SBG
1980	F1536	111	3	0.0202	2.30	...	0.97	...	16.68	178.403	-0.3745	-0.5838	SBG
1985	F1536	111	3	0.0193	1.99	...	1.18	0.59	16.35	242.643	...	-0.3483	-0.4310	-0.8509	SBG
1994	F1536	111	3	0.0190	1.81	...	3.46	...	39.57	273.290	-0.3488	-0.6364	SBG
2009	F1541	1423	111	2	0.0363	1.08	10.37	1.75	69.56	311.687	...	-0.7644	-0.4166	-0.6688	SBG
2035	F1549	7857	111	3	0.0351	4.05	1.88	14.75	18.65	221.163	...	0.5453	-0.1714	-1.4050	Sy2
2049	F1549	3255	112	1	0.0359	1.19	6.96	1.84	8.47	120.138 ^c	...	-0.6179	-0.3379	-0.6329	SBG
2059	F1553	4183	151	2	0.0405	1.76	2.49	9.65	7.79	117.068	...	0.5218	-0.2089	-0.5984	LIN
2073	F1602	6152	111	1	0.0718	0.45	13.95	98.79	73.77	110.487	...	0.8190	-0.3462	-0.2977	Sy2
2081	F1602	3982	112	3	0.0244	1.22	1.67	0.86	12.52	63.050 ^c	...	-0.2941	-0.4139	-0.6104	SBG
2098	F1606	6173	111	2	0.0439	3.01	0.74	11.72	46.60	149.876	...	1.0732	-0.0630	-0.8461	Sy1
2106	F1606	2707	112	3	0.0598	3.25	0.26	0.19	3.07	47.662 ^c	...	-0.2232	-0.2385	-0.5051	SBG
2125	F1610	5338	111	1	0.0252	0.69	18.44	14.63	99.86	384.278	...	-0.0806	-0.5667	-0.5242	SBG
2129	F1610	4971	111	2	0.0594	1.04	5.29	32.25	45.61	65.932	...	0.7484	-0.0760	-0.5073	Sy2
2130	F1610	2764	111	3	0.0718	2.16	0.99	0.43	17.48	57.137	...	-0.3953	-0.2958	-0.4768	SBG
2145	F1615	3766	111	3	0.0805	1.50	1.63	...	17.84	94.021	-0.4016	-0.5820	SBG
2148	F1615	4345	111	3	0.0549	1.10	4.04	1.01	27.78	92.396	...	-0.5716	-0.2327	-0.5536	SBG

^a In units of 10⁻¹⁶ ergs s⁻¹ cm⁻².

^b In logarithmic units.

^c Observation made under nonphotometric conditions.

TABLE 4
MDM SPECTROSCOPIC DATA: 30° BLUE SURVEY

KISSB (1)	FIELD (2)	ID (3)	RUN (4)	Q (5)	z (6)	c _{Hβ} (7)	EW (Å)					FLUX RATIO ^b					TYPE (17)
							[O III] (8)	Hβ (9)	[O III] (10)	Hα (11)	Hα FLUX ^a (12)	[O III]/Hβ (13)	[O III]/Hβ (14)	[N III]/Hα (15)	[S III]/Hα (16)		
1	F0830	3627	151	1	0.0072	0.47	28.43	22.06	23.22	678.504 ^c	...	-0.1300	-0.6876	-0.6998	SBG	
4	F0835	512	152	1	0.0650	1.24	6.16	89.18	6.78	92.376 ^c	...	1.1190	-0.0373	-0.3286	Sy2	
5	F0840	2654	153	1	0.0278	0.87	9.22	32.22	16.07	242.086	...	0.5146	-0.4336	-0.3117	SBG	
7	F0840	1557	153	1	0.0186	0.50	12.74	57.98	65.67	93.068	...	0.6031	-1.2369	-0.6236	SBG	
10	F0845	144	152	1	0.0273	0.78	11.92	61.54	40.80	234.003 ^c	...	0.6626	-0.7105	-0.4499	SBG	
16	F0905	3069	152	1	0.0644	0.57	10.49	23.34	32.97	100.218 ^c	...	0.3255	-0.7073	-0.4712	SBG	
19	F0910	1396	153	1	0.0137	0.72	11.08	23.99	46.44	242.803	...	0.3200	-0.7773	-0.5910	SBG	
20	F0925	2132	152	1	0.0761	0.33	48.87	127.50	124.80	184.092 ^c	...	0.3814	-0.8523	-0.6765	SBG	
22	F0935	3726	152	1	0.0059	0.55	11.24	31.84	37.25	126.910 ^c	...	0.4327	-0.9029	-0.4848	SBG	
23	F0935	158	152	1	0.0016	0.38	21.40	54.72	111.80	106.032 ^c	...	0.3633	-1.3691	-0.8869	SBG	
24	F0940	2414	153	2	0.0281	0.26	21.81	82.28	68.19	42.194	...	0.5456	-1.2705	-0.5484	SBG	
28	F0940	146	152	1	0.0316	Gal	
29	F1005	3849	152	1	0.0044	0.38	17.31	39.03	46.57	327.019 ^c	...	0.3331	-0.7889	-0.6240	SBG	
30	F1005	3288	153	2	Star	
32	F1005	2436	151	1	0.0508	1.05	5.30	44.51	9.13	146.656 ^c	...	0.8854	-0.1210	-0.4219	Sy2	
42	F1055	125	153	1	0.0028	0.01	37.74	128.60	104.90	165.963	...	0.4835	-0.9731	-0.8295	SBG	
46	F1100	802	153	1	0.0522	0.26	12.40	26.71	38.37	69.980	...	0.3018	-0.7265	-0.4468	SBG	
47	F1100	449	151	1	0.0024	0.12	70.91	392.00	312.20	1286.307 ^c	...	0.7100	-1.7924	-1.1560	SBG	
56	F1115	3402	152	3	0.0299	0.58	0.57	0.78	0.22	10.017 ^c	...	0.1256	0.2397	-0.1294	Gal	
57	F1115	3183	152	2	0.0234	0.76	7.15	9.00	27.25	121.156 ^c	...	0.0708	-0.5479	-0.4788	SBG	
58	F1115	1944	153	1	0.0235	1.76	11.58	69.36	130.60	723.700	...	0.7193	-0.7877	-0.9377	Sy1	
62	F1120	3321	153	1	0.0480	1.08	14.56	49.16	27.17	334.497	...	0.4934	-0.4674	-0.5531	SBG	
65	F1125	2024	153	2	0.0075	0.66	12.93	56.82	46.69	83.661	...	0.6066	-1.0511	-0.7120	SBG	
74	F1145	1838	152	1	0.0555	0.48	111.20	1055.00	293.00	61.554 ^c	...	0.7900	-1.3945	-0.9695	SBG	
77	F1145	1144	153	3	0.0223	4.85	1.23	76.880	0.0535	-0.1681	LIN	
93	F1215	1627	22	1	0.0752	0.32	31.00	127.90	177.30	453.743	...	0.6122	-1.0961	-0.959	SBG	
96	F1225	1225	153	1	0.0821	0.43	60.75	56.53	259.50	351.900	...	-0.0439	...	-1.5303	Sy1	
98	F1230	2407	151	2	0.0018	0.20	94.54	421.20	698.30	49.694	...	0.6229	-1.5308	-0.9456	SBG	
99	F1230	1857	32	1	0.0279	0.62	7.14	15.35	44.62	180.926	...	0.3346	-0.7258	-0.4859	SBG	
109	F1250	407	32	2	0.0078	0.07	24.89	18.35	49.82	23.210	...	0.1042	-0.6698	-0.5713	SBG	
120	F1305	6848	21	2	0.0185	1.11	3.61	13.86	26.99	12.290	...	0.5568	-0.9505	-0.3116	SBG	
121	F1305	5813	21	1	0.0267	0.29	137.90	575.60	853.00	585.481	...	0.5941	-1.2290	-0.8514	SBG	
122	F1305	4752	22	1	0.0161	0.40	11.82	27.50	62.22	231.200	...	0.3713	-0.9380	-0.5265	SBG	
123	F1305	3684	21	1	0.0175	0.39	11.16	44.92	59.66	85.100	...	0.6244	-1.2829	-0.7424	SBG	
124	F1305	2967	21	2	0.0247	1.99	2.97	9.03	47.89	24.280	...	0.4448	-1.2717	-0.4659	SBG	
125	F1305	2697	21	3	0.0206	16.65	21.43	9.752	-0.7692	-0.3633	SBG	
126	F1305	2217	21	1	0.0396	0.40	14.85	43.90	79.23	39.210	...	0.4511	-1.3506	-0.6260	SBG	
127	F1305	167	21	1	0.0842	0.16	44.49	222.90	208.70	72.583	...	0.7172	-1.1737	-0.9005	SBG	
131	F1320	262	23	1	0.0726	1.19	23.29	15.44	152.90	337.518 ^c	...	-0.2325	Sy1	
132	F1320	226	31	1	0.0233	0.88	3.00	42.59	16.54	54.050	...	1.1382	0.0104	-0.2473	Sy2	
133	F1325	3189	23	1	0.0172	0.39	61.63	281.90	296.00	1021.117 ^c	...	0.6411	-1.2712	-0.8685	SBG	
138	F1335	3744	31	1	0.0029	0.31	6.47	19.00	35.11	118.000	...	0.4801	-1.2845	-0.5970	SBG	
142	F1345	3363	22	1	0.0766	0.71	28.76	20.35	181.50	118.000	...	-0.1811	...	-1.3903	Sy1	
145	F1355	4898	23	1	0.0076	-0.02	48.76	212.90	226.30	592.871 ^c	...	0.6362	-1.5771	-0.9326	SBG	
146	F1355	4736	151	1	0.0369	0.24	94.69	276.50	124.70	79.889	...	0.3464	-0.8895	-0.7210	SBG	

TABLE 4—Continued

KISSB (1)	FIELD (2)	ID (3)	R _{UN} (4)	Q (5)	z (6)	c _{Hβ} (7)	EW (Å)				FLUX RATIO ^b					TYPE (17)
							[O III] (8)	Hβ (9)	[O III] (10)	Hα (11)	Hα FLUX ^a (12)	[O III]/Hβ (13)	[O III]/Hβ (14)	[N III]/Hα (15)	[S III]/Hα (16)	
149.....	F1400	4177	23	1	0.0274	0.44	...	32.12	47.23	147.50	783.691 ^c	...	0.1748	-0.6807	-0.7941	SBG
158.....	F1415	5070	23	1	0.0856	1.07	...	4.09	19.02	23.10	108.864 ^c	...	0.6422	-0.1055	-0.2063	Sy2
161.....	F1415	3598	23	1	0.0110	0.54	...	6.07	26.12	38.23	154.333 ^c	...	0.6194	-1.3919	-0.6052	SBG
162.....	F1415	3127	23	1	0.0354	0.44	...	22.92	38.62	130.80	265.202 ^c	...	0.1847	-0.7240	-0.5206	SBG
167.....	F1425	46	31	1	0.0121	-0.15	...	34.97	69.38	100.20	28.340	...	0.4749	-1.2391	-0.7104	SBG
176.....	F1450	3971	153	2	0.0589	1.29	...	1.76	31.46	2.26	40.941	...	1.2016	-0.0174	-0.1786	Sy2
180.....	F1500	3752	152	1	0.0715	0.74	...	13.23	15.22	31.12	113.569	...	0.0415	-0.5880	-0.5085	SBG
183.....	F1510	4905	153	3	0.0584	1.34	...	2.39	1.28	7.05	41.599	...	-0.3215	-0.3323	-0.5913	SBG
185.....	F1515	5655	153	1	0.0871	0.33	...	47.23	212.90	117.00	101.007	...	0.5929	-1.1721	-0.7359	SBG
186.....	F1515	5729	32	1	0.0332	0.11	...	133.50	890.10	807.90	107.300	...	0.8110	-2.0621	-1.4086	SBG
189.....	F1520	2625	23	2	0.0229	1.17	...	5.00	0.97	35.80	361.210 ^c	...	-0.7389	-0.4223	-0.7001	SBG
191.....	F1520	1404	23	1	0.0868	1.26	...	9.80	134.80	78.10	373.921 ^c	...	1.1003	-0.0016	-0.2511	Sy2
204.....	F1600	3730	32	1	0.0319	0.41	...	20.26	84.27	117.90	169.800	...	0.6206	-1.4019	-0.7023	SBG
205.....	F1605	7625	23	1	0.0311	0.51	...	16.45	21.32	85.75	346.589 ^c	...	0.1200	-0.7543	-0.5006	SBG
209.....	F1610	7809	21	1	0.0419	0.55	...	17.34	47.17	96.20	95.843	...	0.4126	-0.8314	-0.6478	SBG
211.....	F1615	4535	23	2	0.0247	-0.07	...	32.22	82.14	95.33	51.569 ^c	...	0.4453	-1.8206	...	SBG
218.....	F1650	8621	31	1	0.0327	0.54	...	19.37	31.62	113.20	629.200	...	0.2095	-0.7570	-0.7223	SBG

^a In units of 10^{-16} ergs s^{-1} cm^{-2} .

^b In logarithmic units.

^c Observation made under nonphotometric conditions.

TABLE 5
KISSB-KISSR ID COMPARISON

KISSB (1)	KISSR (2)	Field (3)	ID (4)
93.....	12	F1215	1627
96.....	67	F1225	1225
99.....	76	F1230	1857
109.....	146	F1250	407
120.....	192	F1305	6848
121.....	196	F1305	5813
122.....	202	F1305	4752
123.....	205	F1305	3684
124.....	207	F1305	2967
125.....	210	F1305	2697
126.....	212	F1305	2217
127.....	223	F1305	167
131.....	281	F1320	262
132.....	282	F1320	226
133.....	286	F1325	3189
138.....	314	F1335	3744
142.....	350	F1345	3363
146.....	401	F1355	4736
149.....	421	F1400	4177
158.....	497	F1415	5070
161.....	505	F1415	3598
162.....	509	F1415	3127
167.....	561	F1425	46
176.....	584	F1450	3971
180.....	621	F1500	3752
183.....	651	F1510	4905
185.....	665	F1515	5655
189.....	707	F1520	2625
204.....	955	F1600	3730
205.....	964	F1605	7625
209.....	985	F1610	7809
218.....	1094	F1650	8621

two categories represent objects that were mistakenly identified by the survey as ELGs; they are not actual extragalactic emission-line sources. Note that all objects whose spectra indicate photoionization by hot stars are cataloged as SBGs, regardless of their nature. We do not attempt to classify SBGs into other subcategories of star-forming galaxies (e.g., blue compact dwarfs, H II galaxies, etc.), since such classifications are both highly subjective and are dependent on the type of data used.

Note that Tables 2 and 4 contain data for a number of objects in common (see Table 5). Since KR1 and KB1 overlap in terms of sky coverage, many ELG candidates are detected in both surveys (which use independent spectral data). It was decided to include the spectral data for the objects that are duplicated in the two survey lists in both data tables. This way, a reader attempting to locate information about a specific KISSB object will not be forced to cross-check the KB1 catalog with KR1.

To illustrate the range of objects identified by KISS, some characteristic spectra of objects observed with the MDM 2.4 m telescope are presented in Figures 1–5. Three starburst galaxy spectra of different Q values show the range of spectral quality in the sample (Fig. 1). Figure 2 shows three starburst galaxies with varying degrees of ionization, as indicated by the $[\text{O III}]\lambda 5007/\text{H}\beta$ ratio. Figures 3 and 4 show example spectra of Seyfert 1 and Seyfert 2 galaxies. One Seyfert 1 and one Seyfert 2 galaxy lie at moderate red-

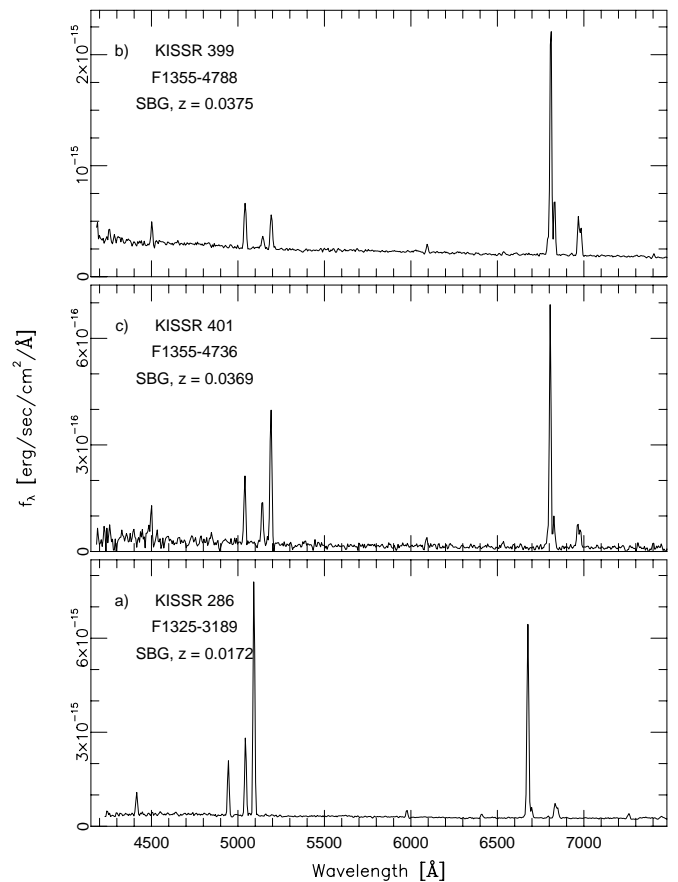


Fig. 2.—Sample MDM spectra of starburst galaxies. All have spectral quality $Q = 1$. The spectra are ordered by increasing degree of excitation, as shown by their $[\text{O III}]\lambda 5007/\text{H}\beta$ ratios. As $[\text{O III}]\lambda 5007/\text{H}\beta$ increases, $[\text{N II}]/\text{H}\alpha$ and $[\text{S II}]/\text{H}\alpha$ decrease. (a) Low-excitation starburst: $[\text{O III}]\lambda 5007/\text{H}\beta \sim 0.8$ and $[\text{N II}]/\text{H}\alpha \sim 0.2$. (b) Medium-excitation starburst: $[\text{O III}]\lambda 5007/\text{H}\beta \sim 2$ and $[\text{N II}]/\text{H}\alpha \sim 0.1$. (c) This high-excitation starburst spectrum has $[\text{O III}]\lambda 5007/\text{H}\beta \sim 4$, similar to what is seen for many Seyfert 2 galaxies. However, its $[\text{N II}]/\text{H}\alpha$ ratio is only ~ 0.05 .

shift ($z \sim 0.3$); they exemplify the objects identified by the H α -selected red survey where another emission line ($[\text{O III}]\lambda 5007$ in both cases) is redshifted into the H α region. About 2% of the KISS galaxies with follow-up spectra fall into this category, most of them AGN. Finally, Figure 5 shows the range of spectral characteristics found among the objects we classify as LINERs. A more complete discussion of the AGN population found in the KISS catalogs is given in Gronwall, Sarajedini, & Salzer (2002) and Stevenson et al. (2002).

3.2. Classification

Emission-line objects detected by KISS span a wide range of object types, from star-forming dwarf galaxies to AGN. The survey objective-prism spectra cannot be used to classify the objects according to the nature of the source of the ionizing radiation; their resolution is too low, and they cover only the spectral range 6400–7200 Å. (See KR1, Fig. 2 for some examples of objective-prism spectra). It is, however, often possible to make a tentative classification of an ELG simply by looking at its long-slit spectrum. Seyfert 1 galaxies, for instance, are easily recognized from the broadening of their permitted lines. The MDM spectra have the lowest dispersion of all the spectroscopic follow-up

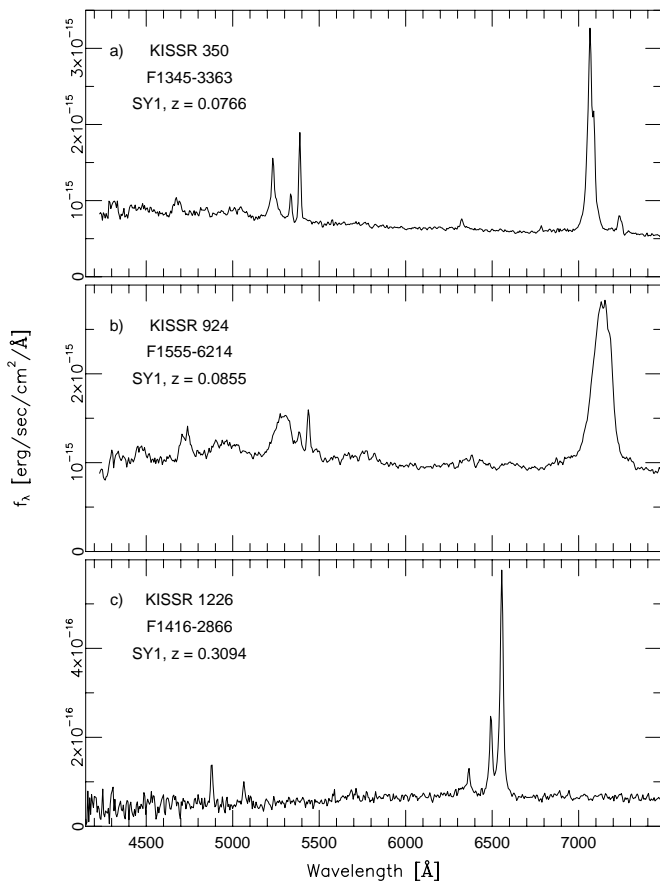


FIG. 3.—Sample MDM spectra of Seyfert 1 galaxies. All have spectral quality $Q = 1$. (a) In this spectrum, both a narrow and a broadened hydrogen line component can be seen. (b) The narrow forbidden lines are mostly hidden by the strongly broadened hydrogen lines. (c) In this moderate- z object, the strongest lines are $H\beta$ and the $[O III]$ doublet.

observations, causing the $[N II]\lambda 6583$ line to blend with $H\alpha$ and the $[S II]\lambda\lambda 6717, 6731$ doublet to be blended as well. Still, the dispersion is high enough for ELG classification (see Figs. 2–5) and for the measurement of crucial emission-line ratios.

The line ratios allow us to plot diagnostic diagrams that give a clear separation of different types of ELGs (see, e.g., Baldwin, Phillips, & Terlevich 1981; Veilleux & Osterbrock 1987). The location of each object in the diagram is used to assign the activity type classification listed in Tables 2–4. In Figure 6, we plot $\log([O III]\lambda 5007/H\beta)$ against $\log([N II]\lambda 6583/H\alpha)$ for all MDM sample objects classified as starburst galaxies or AGNs with follow-up spectra of quality code $Q = 1$ or 2. As expected from models for starburst-powered ELGs of various metallicities, most objects fall along a sequence that arcs across the diagram. The solid line indicates the positions of $H II$ region models of different metallicities (Dopita & Evans 1986). Low-metallicity starbursts are found in the top left portion of the diagram, high-metallicity starbursts in the bottom right. Objects powered by an active galactic nucleus (AGN)—Seyfert 2 galaxies and (presumably) LINERs—have higher values of $[N II]\lambda 6583/H\alpha$ and are located in the top right portion of the diagram. Not included in the diagram are the moderate-redshift AGN, since their observed spectra lack the $[N II]\lambda 6583/H\alpha$ ratio (their $H\alpha$ and $[N II]$ lines were redshifted out of our spectral range).

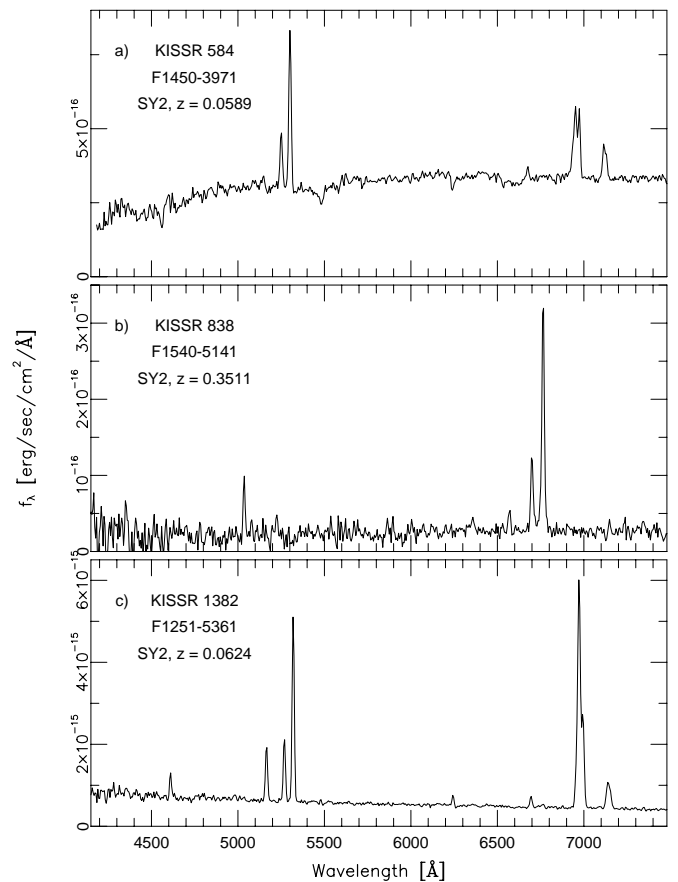


FIG. 4.—Sample MDM spectra of Seyfert 2 galaxies. (a) In this $Q = 2$ spectrum, $H\alpha$ and $[N II]\lambda 6583$ are of equal strength; $H\beta$ is so weak that it is difficult to measure. Several absorption features are clearly visible. (b) A moderate- z object with $Q = 2$, where the strongest lines belong to the $[O III]$ doublet. The $[O III]/H\beta$ ratio is much higher than for most star-forming objects; $[O III]/H\beta \sim 8$. In the blue region of the spectrum, $[O II]\lambda\lambda 3726, 3729$ is visible. (c) This $Q = 1$ spectrum shows a borderline object with $[O III]/H\beta \sim 3.3$ and $[N II]/H\alpha \sim 0.4$. The strength of the $[O I]\lambda 6300$ line indicates that the object is an active galaxy.

Of the 351 objects with follow-up spectra obtained at MDM, the majority (268, or 76%) are classified as SBGs of some type. This category includes a diverse range of star-forming galaxies, such as starburst nuclei galaxies, $H II$ galaxies, irregular galaxies with significant star formation, and blue compact dwarfs. Since KISS detects a significant number of objects with $H\alpha + [N II]$ emission-line equivalent widths smaller than 30 \AA , the SBG class will also include some intermediate- to late-type spiral galaxies (Kennicutt & Kent 1983; Kennicutt 1992). Active galaxies make up nearly 20% of the sample: nine objects (2.5%) are Seyfert 1 galaxies, 31 (9%) are Seyfert 2 galaxies, 25 (7%) are LINERs, and one is a QSO at $z = 0.46$. As we describe above, this large fraction of active galaxies is due, at least in part, to the specifics of the sample selection for the MDM spectral observations.

The remaining 17 objects (5%) are non-ELGs: 10 are Galactic stars, and seven are galaxies with no emission lines in the wavelength region included in the objective-prism spectra. To date, our follow-up spectroscopy has shown that $\sim 7\%$ of the objects cataloged in KISS are actually non-ELGs. A comparison of their survey properties shows that the objective-prism fluxes of non-ELGs are lower than for the bulk of the confirmed ELGs, and their $B-V$ colors tend

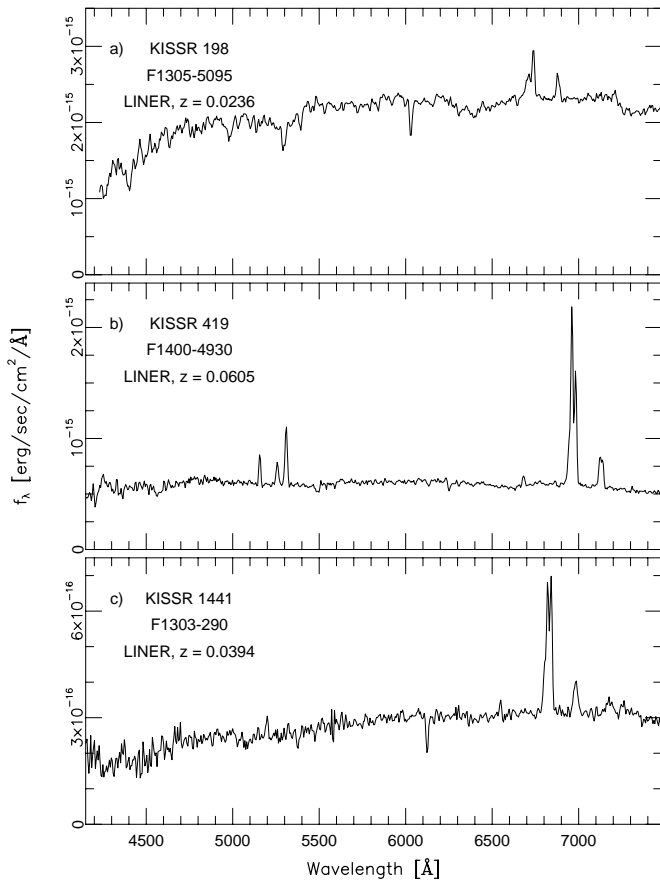


FIG. 5.—Sample MDM spectra of LINERs. (a) Only $H\alpha$, $[N\ II]$, and $[S\ II]$ can be measured in this $Q = 3$ spectrum. The $[N\ II]\lambda 6583$ line is twice as strong as $H\alpha$. Absorption features associated with $H\beta$, $Mg(\lambda 5175)$, and $Na(\lambda 5892)$ are evident. (b) In this $Q = 1$ spectrum, $H\beta$ and the $[O\ III]$ doublet can be seen as well as $H\alpha$, $[N\ II]$, and $[S\ II]$. (c) In this $Q = 2$ spectrum, $H\alpha$ and $[N\ II]$ are of comparable strength. $Na(\lambda 5892)$ absorption can be seen.

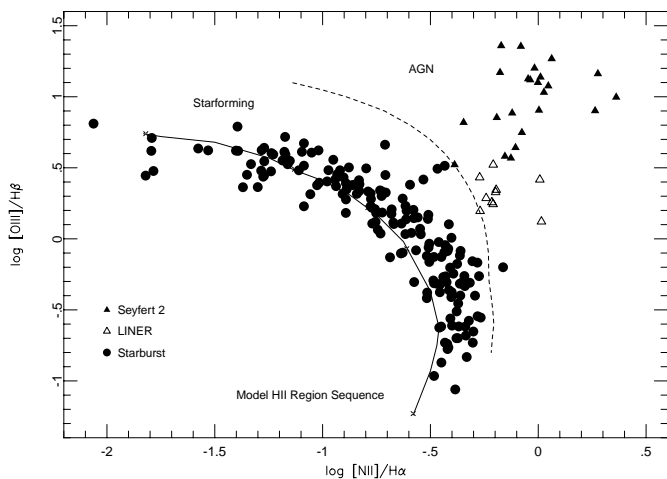


FIG. 6.—Line diagnostic diagram showing the relationship between the $[N\ II]\lambda 6583/H\alpha$ line ratio and the $[O\ III]\lambda 5007/H\beta$ line ratio. Only objects with spectral quality of $Q = 1$ or 2 were included in the diagram. Objects classified as SBG are shown as filled circles, LINERs as open triangles, and Seyfert 2 galaxies as filled triangles. The dashed line (from Veilleux & Osterbrock 1987) roughly separates the star-forming galaxies from the active galaxies. The solid line represents an $H\ II$ model sequence at various metallicities, from $0.1 Z_{\odot}$ at the top left to $2 Z_{\odot}$ at the bottom right (Dopita & Evans 1986).

to be redder; roughly half the sources with $B - V > 1.1$ are non-ELGs. The sources that are confirmed to be ELGs also tend to have brighter magnitudes than the non-ELG sources. For confirmed ELGs the median magnitude is $B \sim 17.8$, while for non-ELGs it is only $B \sim 19.4$. The ELGs and non-ELGs have similar distributions of objective-prism equivalent widths and redshifts. A more complete discussion of the properties of the false detections will be given in Gronwall et al. (2003a).

3.3. Properties of an Unbiased Subsample of KISS ELGs

The follow-up observations obtained at MDM and other telescopes offer us the opportunity to study in greater detail the spectroscopic characteristics of the ELG population detected by KISS. In each survey field observed at MDM, we obtained follow-up spectra of a varying fraction of the ELG candidates. As described in § 2.1, the selection of these targets was not random. We thus need to evaluate what effects the target selection has on the observed spectral properties. To facilitate this evaluation, *all* ELG candidates in two of the survey fields (F1305 and F1610) were observed—a total of 56 objects (hereafter, the random sample). While the objects observed in all other survey fields represent a biased sample of KISS ELGs, the objects in these two randomly chosen fields should be representative of the KISS ELGs in general. We have verified that the objects in the random sample have the same overall characteristics, as determined from objective-prism data, as the objects in the total survey database; their median $B - V$ colors, $H\alpha$ line fluxes, and equivalent widths are all comparable. Objects in the random sample have median apparent magnitudes that are ~ 0.5 mag brighter than what is seen for the entire survey; however, their median absolute magnitudes are fainter by ~ 0.3 mag. The explanation for this is that the random sample ELGs tend to lie at lower redshifts. The median redshift for the random sample is only $z \sim 0.04$, while for the entire KISS database the median redshift is $z \sim 0.06$. This difference in redshift is caused by the fact that the Coma Cluster (at $z \sim 0.02$) is partially included in survey field F1305.

In survey fields other than the two completely observed fields, the targets for MDM spectroscopy were chosen based on various criteria. These observations produced a sample of 295 objects that we will refer to as the selected sample. When comparing the properties (determined from the follow-up spectra) of the ELGs in the random sample to those of ELGs in the selected sample, the most significant difference we find is that starburst galaxies make up a much greater fraction of the random sample—50 out of the 56 ELG candidates (89%) are classified as SBGs. Only four objects representing different types of active galaxies were found, thus AGN account for only 7% of the sample. The remaining two objects are a Galactic star and a galaxy without emission lines. Due to the way targets were chosen for follow-up observations, AGN are overrepresented in the selected sample, where they account for 20% of the observed sources. For comparison, only 10% of the 30° Red Survey sample (where we have follow-up spectra for 67% of the 1128 sources) are classified as active galaxies. If the random sample is indeed representative of the KISS ELG population, we expect that the fraction of AGN in the survey will drop below 10% as we obtain and analyze follow-up spectra for the remaining ELG candidates.

Furthermore, we find that the selected sample has a lower median $H\alpha$ equivalent width than the random sample. This is most likely an effect of the larger fraction of AGN (which generally have lower equivalent widths than SBGs) in the selected sample. Yet another effect of the different makeup of the two samples is seen when we compare their reddening coefficients ($c_{H\beta}$). As expected, the reddening of the AGN-rich selected sample is significantly higher (median $c_{H\beta} = 0.89$) than that of the SBG-dominated random sample (median $c_{H\beta} = 0.66$).

The random and selected samples also show differences between their $H\alpha$ line fluxes. The random sample has a lower median line flux, $4 \times 10^{-15} \text{ ergs s}^{-1} \text{ cm}^{-2}$, than the selected sample, which has a median line flux of $6.8 \times 10^{-15} \text{ ergs s}^{-1} \text{ cm}^{-2}$. This is mainly caused by the preference given to objects with high $H\alpha$ luminosities when selecting targets for follow-up spectroscopy. The selection of sources with bright absolute magnitudes also contributed to a bias toward targets with higher line fluxes.

To summarize, the differences found between the random and selected samples highlight the effects of the target selection procedure. The full sample of objects observed at MDM is dominated by selected objects, and thus their spectral properties should not be seen as representative of the ELG population detected by KISS. The sample of random objects, while small, gives an indication of what general characteristics we can expect to find for the overall collection of KISS objects.

4. COMPARISON OF SURVEY AND FOLLOW-UP SPECTROSCOPIC PROPERTIES

The KISS database contains a wealth of information for a large sample of ELG candidates and can potentially be used for a wide range of galaxian studies. The objective-prism spectral data, however, are inherently uncertain: their resolution is low, and they cover only a limited spectral range. How reliable are the redshifts, line fluxes, and equivalent widths that we derive from the survey data? For objects with follow-up spectroscopy, we can attempt to answer this question by comparing the objective-prism measurements to their long-slit counterparts.

Based on the KISS objective-prism data, redshifts have been estimated for all survey sources. The follow-up spectroscopy made it possible to check how well the prism redshifts correspond to redshifts obtained from higher resolution slit spectra. Figure 7 shows a comparison of the two redshifts. The overall agreement is good; out of the 351 objects observed, only 17 were found to have redshifts substantially different from the prism estimates ($\Delta v > \pm 4000 \text{ km s}^{-1}$). Eight of these were cases where a strong $[O\text{ III}]\lambda 5007$ or $H\beta$ line of an AGN at $z = 0.3\text{--}0.5$ was redshifted to the bandpass covered by the red KISS objective-prism data and was misinterpreted as $H\alpha$ from a nearby dwarf galaxy (see Fig. 7*b*). Unfortunately, the only way to distinguish these cases is through follow-up spectroscopy, since the resolution of the objective-prism spectra is too low to allow us to discriminate between the two options. A further six objects that were initially identified as extragalactic objects at $z = 0.02\text{--}0.08$ were found to be Galactic stars. The remaining three objects are galaxies without emission lines that were included as ELG candidates due to spurious features or noise. For all other objects, where the objective-prism redshift is actually based on an $H\alpha$ detection, the

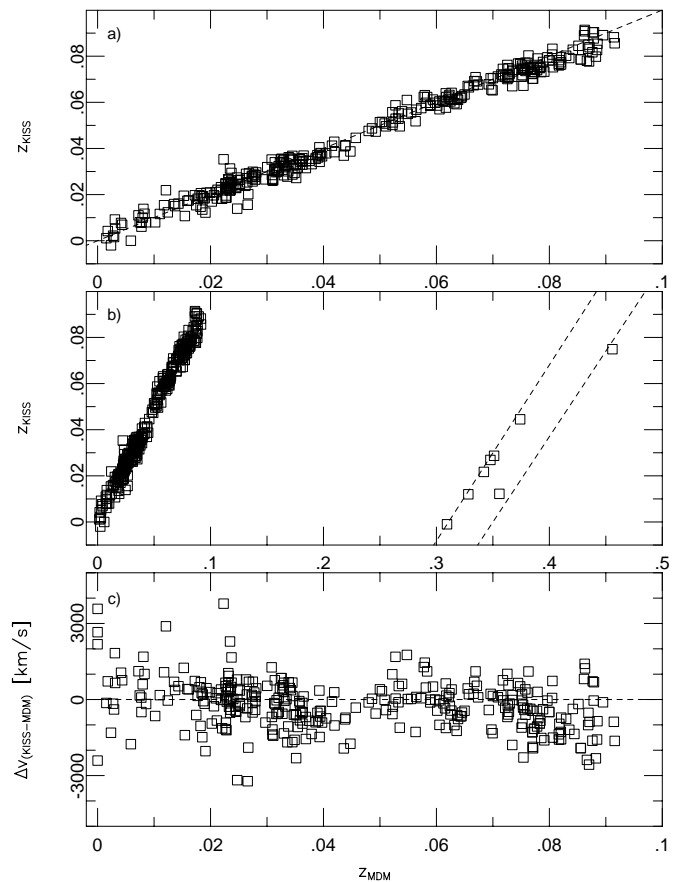


Fig. 7.—Comparison of objective-prism redshifts to long-slit redshifts. Objects determined to be Galactic stars or non-ELGs have been excluded from the plots. (a) Overall there is good agreement between objective-prism redshifts (z_{KISS}) and the redshifts determined from the follow-up long-slit spectroscopy (z_{MDM}). (b) The dashed lines in the right portion of the diagram show the expected positions of objects for which either $[O\text{ III}]\lambda 5007$ (left line) or $H\beta$ (right line) of a moderate-redshift source were misidentified as $H\alpha$ emission in the objective-prism spectra. Six objects were detected by the survey due to their strong $[O\text{ III}]\lambda 5007$ line, and two were detected from their $H\beta$ line. (c) Above $z_{\text{MDM}} = 0.07$, the effect of the survey filter cutoff becomes apparent: the objective-prism redshifts are systematically lower than the long-slit redshifts, and this difference increases with redshift.

prism redshifts are comparable to those determined from the follow-up spectra.

Objects with redshifts $z > 0.07$, close to the filter-imposed redshift limit, tend to have objective-prism redshifts that are systematically lower than the redshifts determined from their long-slit spectra. As can be seen in Figure 7*c*, the difference increases with redshift. This effect arises when the broad line in the objective-prism spectrum falls near the wavelength cutoff of the survey filter: only the shorter wavelength part of the line will then be detected, giving the impression of a weaker line at lower redshift. As described in Paper I, a correction for this effect was applied to the high-redshift portion of the first red survey list (KR1).

Using the corrected objective-prism redshifts, and including only those objects whose KISS redshifts were based on the detection of the $H\alpha$ line, we find that the velocity difference Δv has a scatter of $\sigma = \pm 965 \text{ km s}^{-1}$. This number is consistent with expectations based on the accuracy of the objective-prism redshifts, for which the dispersion is $24 \text{ \AA pixel}^{-1}$ at $H\alpha$. The prism-estimated redshifts tend to be slightly lower than their counterparts measured with a slit,

corresponding to a velocity difference of $\sim 30 \text{ km s}^{-1}$. This offset is very small compared with the scatter—only 0.03σ .

We compared the redshifts of 129 objects that have data from both MDM long-slit spectroscopy and Century Redshift Survey observations (CRS; Wegner et al. 2001). The two data sets show good agreement, with no apparent systematics. The MDM redshifts are slightly higher than the CRS redshifts, but the median offset is only 7.8 km s^{-1} . The standard deviation is $\sim 90 \text{ km s}^{-1}$. It should be noted that the CRS redshifts were not determined from the emission lines alone: the software used to extract the redshifts also employed a cross-correlation algorithm for the absorption-line features (Thorstensen et al. 1989). The CRS redshifts can thus in some cases be independent of the emission-line features.

The telluric $\text{O}_2 B$ band may also be causing a systematic offset in the prism redshift for objects where the $\text{H}\alpha$ line falls in the region of this absorption feature. The position of the B band (6860–6890 Å) corresponds to an $\text{H}\alpha$ redshift of 0.045–0.050. We would expect the measured prism redshift to be shifted blueward for objects with redshifts in the range $0.040 < z < 0.0475$ and redward for objects at $0.0475 < z < 0.055$. A hint of this behavior appears to be present in Figure 7c; however, comparison to the CRS redshift data do not show the deviations to be statistically significant. We also might expect fewer objects to be detected at the center of the B band, since absorption would cause objects with weak emission lines to fall below the detection threshold of the survey. We do see fewer objects in this redshift range; however, a deficit of objects is expected, since a large void is located at $0.038 < z < 0.054$. For comparison, we selected the 1028 CRS objects that lie in the range of right ascension that overlaps with the KISS database (R.A. = $12^{\text{h}}15^{\text{m}}\text{--}16^{\text{h}}28^{\text{m}}$, excluding objects between $14^{\text{h}}30^{\text{m}}$ and $14^{\text{h}}45^{\text{m}}$). In the redshift range of the B band, the number of CRS objects drops by 30% with respect to the number of objects in the region on the near side of the void ($0.23 < z < 0.38$). For the 1034 KISS objects in the same right ascension range, the drop is more precipitous: 64% fewer objects are detected between $z = 0.040$ and 0.055 . This could be due to B -band absorption, but the coincident position of the void makes it difficult to verify.

We also wished to see how well the $\text{H}\alpha$ equivalent widths (EWs) and line fluxes derived from the objective-prism spectra agree with those we measure in the follow-up spectra. For this comparison, we only included the line fluxes of objects for which the follow-up observations were carried out under spectrophotometric conditions. In the low-resolution prism spectra, the $[\text{N II}]$ lines are completely blended with the $\text{H}\alpha$ line, but in the MDM spectra these lines are partly resolved. As described in § 2.3, measurements of the individual line fluxes are possible using a deblending routine. For the purposes of this comparison, we used the $[\text{N II}]\lambda 6583/\text{H}\alpha$ flux ratio determined from the MDM spectra to correct the prism spectra equivalent widths and fluxes, effectively subtracting the $[\text{N II}]$ contribution.

Plotting the $[\text{N II}]$ -corrected objective-prism fluxes versus their long-slit counterparts shows them to be in overall agreement (see Fig. 8a). However, the line fluxes that we estimated from objective-prism spectra are generally $\sim 50\%$ higher than those we measure in the MDM long-slit spectra. Since the objective-prism spectra sample a larger spatial region than the long-slit spectra, it is natural that they will

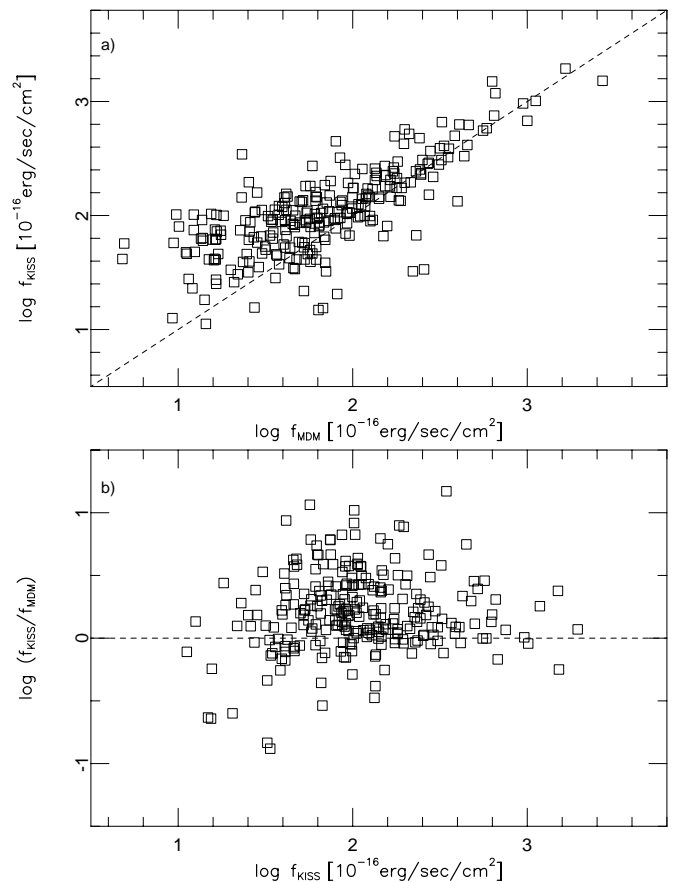


FIG. 8.—Comparison of corrected objective-prism $\text{H}\alpha$ line fluxes, f_{KISS} , to long-slit fluxes, f_{MDM} . (a) The dashed line indicates the relation $f_{\text{KISS}} = f_{\text{MDM}}$. Overall there is a clear correlation between the two, but the objective-prism fluxes tend to be higher than the long-slit fluxes. This is expected since objective-prism spectra include flux from a larger spatial region than the long-slit spectra. (b) This plot shows the line-flux ratio $f_{\text{KISS}}/f_{\text{MDM}}$ vs. f_{KISS} . The dashed line indicates $f_{\text{KISS}}/f_{\text{MDM}} = 1$. In spite of a large scatter, 80% of the sample falls within $0.33 < f_{\text{KISS}}/f_{\text{MDM}} < 3$.

include a greater amount of flux for all extended sources. The objects with the highest objective-prism fluxes show less of an offset from the long-slit fluxes than the bulk of the sample; this could indicate that they correspond to sources with smaller apparent sizes. Plotting the ratio of the two fluxes versus the objective-prism fluxes (Fig. 8b) shows that the objects with the lowest objective-prism fluxes tend to have had their fluxes underestimated.

Comparing the $[\text{N II}]$ -corrected objective-prism equivalent widths to the corresponding long-slit equivalent widths, we see that these too agree reasonably well (see Fig. 9). A weak trend can be seen where sources with low equivalent widths have objective-prism EWs that are higher than their long-slit EWs, while the opposite is seen for sources with high equivalent widths.

A relatively large scatter is evident in the plots of objective-prism equivalent widths and fluxes versus their long-slit counterparts. In the plot comparing objective-prism EWs to the long-slit EWs, we see that the scatter is of the same order as the measured equivalent widths. To some degree, this scatter is to be expected: the spatial extent of the regions from which the spectra are derived is not the same for the two sets of observations. The objective-prism spectra are extracted from a rectangle 4 pixels wide, corresponding to

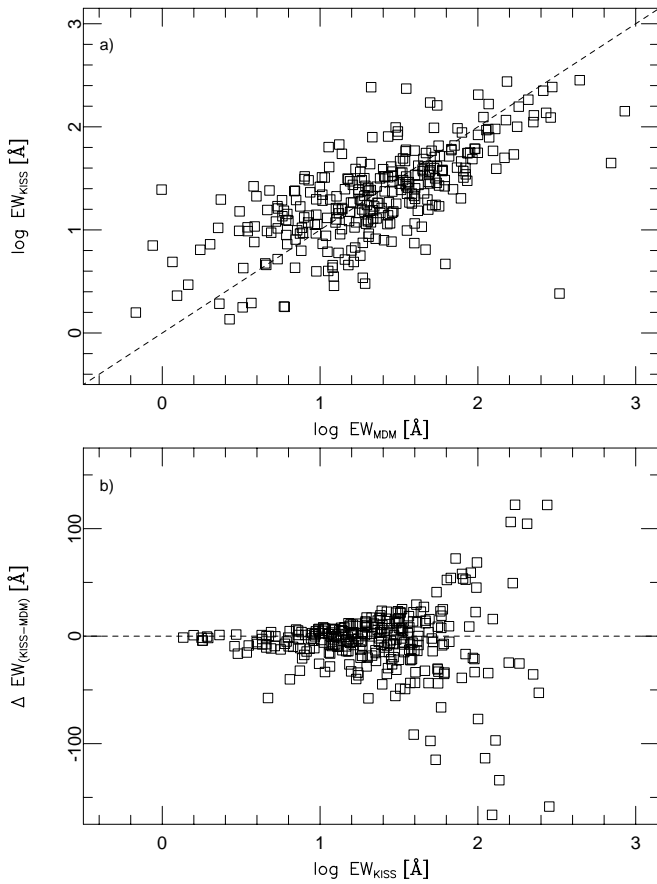


FIG. 9.—Comparison of corrected objective-prism $H\alpha$ equivalent widths (EW_{KISS}) to long-slit equivalent widths (EW_{MDM}). (a) An overall correlation is seen between the two equivalent widths, with no offset toward higher or lower values for either. The dashed line indicates $EW_{KISS} = EW_{MDM}$. Again, since the objective-prism spectra sample a larger spatial region than the long-slit spectra, we do not expect an exact correspondence between equivalent widths measured in each spectra. The difference in distribution of continuum and line emission also greatly affects the equivalent widths. (b) Here we plot the difference in equivalent widths, ΔEW , versus the objective-prism equivalent width EW_{KISS} . The dashed line indicates $\Delta EW = 0$. The EW difference increases for objects with greater EW_{KISS} ; however, the fractional difference $\Delta EW/EW_{KISS}$ remains roughly constant throughout the range of EW_{KISS} .

8", while the MDM slit is only 1"68 wide. When an object that is a point source in both line and continuum emission is observed, the resulting flux and EW should be the same for both spectra, but for extended objects different amounts of line and continuum emission will be detected.

We can combine the comparisons of line fluxes and of equivalent widths to gain some insight into the spatial extent and distribution of the emitting regions within the galaxies. Equivalent width describes the relative strengths of line and continuum emission, while line flux is an absolute measure; a comparison of the results of objective-prism and long-slit spectroscopy will show different signatures depending on the relative size and localization of the regions that emit line and continuum emission. For a spatially resolved object, three simplified scenarios can be invoked when we attempt to explain different results for the comparison of line fluxes and EWs for the two types of spectra. (1) If the line emission comes from a more centrally concentrated region than the continuum emission, we expect the long-slit spectra to show a greater equivalent width than the objective-prism spectra,

since a larger fraction of the continuum emission is excluded by the long-slit spectroscopy. The line flux should be roughly equal for both spectra. (2) In the case where line and continuum emission come from the same region, we expect long-slit and objective-prism equivalent widths to be the same, while line flux should be lower for the long-slit spectra. (3) If continuum emission is more centrally concentrated than line emission (as in the case where there is a ring of star formation in the disk of a galaxy), both the equivalent width and the line flux should be lower in the long-slit spectra. Plotting the difference in equivalent widths (ΔEW) versus the ratio of the line fluxes in Figure 10, we see that the large scatter makes it difficult to check our predictions. However, the objects tend to fall along a line from the bottom left to the top right, which agrees with what we expect. The diagram contains both resolved and unresolved objects; the points that fall close to the center of the diagram likely represent the unresolved objects. The majority of objects further away from the center fall close to the line of $\Delta EW = 0$, $f_{KISS}/f_{MDM} > 1$, corresponding to equal distribution of line and continuum emission. A large fraction of objects are located in the bottom right quadrant, corresponding to cases where the line flux is somewhat more concentrated than the continuum flux. Almost no objects fall in the top left quadrant, which corresponds to relatively higher long-slit flux and lower equivalent width; it is difficult to see how this situation would arise except through mistakes in the spectral reduction.

It is important to note that in spite of the large scatter we see when we compare line fluxes and equivalent widths from the survey database to those from the MDM follow-up observations, the *overall* distribution of these properties is very similar. For example, selecting the objects with (uncorrected) objective-prism line fluxes above the median value

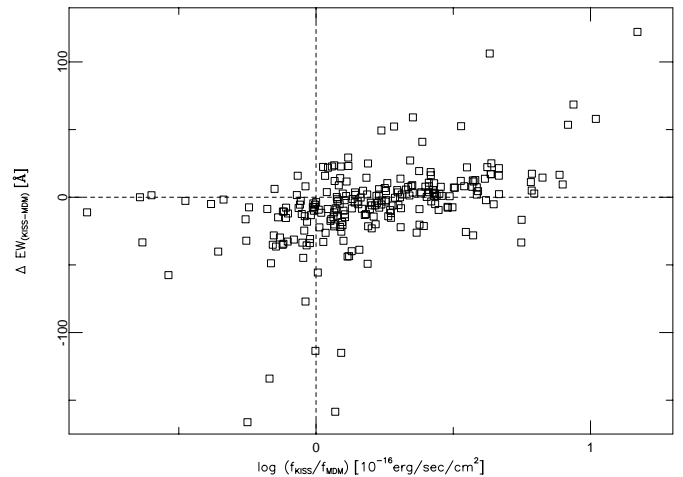


FIG. 10.—Difference in equivalent widths, ΔEW , plotted vs. the ratio of the line fluxes, f_{KISS}/f_{MDM} . The dashed lines represent $\Delta EW = 0$ and $f_{KISS}/f_{MDM} = 1$. Unresolved objects should fall near the intersection of these lines. Since the long-slit spectra sample only the central regions of a resolved object while the objective-prism spectra contain flux from a larger region, differences in the spatial distribution of continuum and line emission of galaxies should be visible in this diagram. We expect galaxies to trace a path from the bottom left (objects with line emission that is more concentrated than their continuum emission) to the top right (objects where the line emission is more extended than the continuum emission). We can see a hint of this trend for the galaxies plotted here, albeit with a large scatter.

of $1.6 \times 10^{-14} \text{ ergs s}^{-1} \text{ cm}^{-2}$ produces a sample that includes $\sim 80\%$ of the high-flux objects as selected from the follow-up observations. The same test for the equivalent widths shows we would include $\sim 75\%$ of the objects found from long-slit spectroscopy to have high EWs if we selected the sample based on the survey EWs.

5. CONCLUSIONS

We present the data from follow-up spectroscopy for a sample of 351 emission-line galaxy (ELG) candidates from the KPNO International Spectroscopic Survey (KISS). This is the first in a series of papers that will present slit spectral data for large numbers of KISS ELGs. We verify that all but 5% of this sample are extragalactic emission-line objects. The long-slit spectra provide redshift information, line fluxes, equivalent widths, and optical reddening estimates. Based on the spectral properties, we have classified the objects as starburst galaxies or various types of active galaxies. Due to the way the follow-up sample was selected, AGN account for nearly 20% of the confirmed ELGs. In two survey fields where all detected sources were observed, only $\sim 7\%$ are classified as AGN.

We have also compared the redshifts, $H\alpha$ line fluxes, and equivalent widths measured in the MDM follow-up spectra

to corresponding data derived from the KISS objective-prism spectra. The objective-prism redshifts of the extragalactic emission-line sources agree well with the redshifts determined from long-slit spectra, except for a small fraction of objects where a blue line had been misidentified as the $H\alpha$ line. The $H\alpha$ fluxes and equivalent widths also show an overall agreement between survey and follow-up data; the scatter that is present is partly due to the fact that the follow-up observations sample different spatial regions of a galaxy.

We gratefully acknowledge financial support for the KISS project from an NSF Presidential Faculty Award to J. J. S. (NSF AST 95-53020), as well as continued support for our ongoing follow-up spectroscopy campaign (NSF AST 00-71114). We also thank Wesleyan University for providing additional funding for the observing runs during which these follow-up spectral data were obtained. We thank Jeff Van Duyne, who participated in one of the observing runs at MDM, and Laura Chomiuk and Kerrie McKinstry, who assisted with the data processing. Finally, we wish to thank Bob Barr of MDM Observatory for his excellent assistance in maintaining the telescope and instrumentation used for these observations.

REFERENCES

- Baldwin, J. A., Phillips, M. M., & Terlevich, R. 1981, *PASP*, 93, 5
 Becker, R. H., White, R. L., & Helfand, D. J. 1995, *ApJ*, 450, 559
 Chomiuk, L. B., Salzer, J. J., & Gronwall, C. 2003, in preparation
 Condon, J. J., Cotton, W. D., Griesen, E. W., Yin, Q. F., Perley, R. A., Taylor, G. B., & Broderick, J. J. 1998, *AJ*, 115, 1693
 Dopita, M. A., & Evans, I. N. 1986, *ApJ*, 307, 431
 Gronwall, C., Salzer, J. J., Jangren, A., Wegner, G. A., Phillips, A. C., Melbourne, J., Ciardullo, R., & McKinstry, K. 2003a, in preparation
 Gronwall, C., Salzer, J. J., Sarajedini, V. L., Jangren, A., Chomiuk, L. B., Moody, J. W., Frattare, L. M., & Boroson, T. A. 2003b, in preparation (KR2)
 Gronwall, C., Sarajedini, V. L., & Salzer, J. J. 2002, in *ASP Conf. Ser.* 284, AGN Surveys, ed. R. F. Green, E. Ye. Khachikian, & D. B. Sanders (IAU Colloq. 184) (San Francisco: ASP), in press
 Kennicutt, R. C. 1992, *ApJ*, 388, 310
 Kennicutt, R. C., & Kent, S. M. 1983, *AJ*, 88, 1094
 Lee, J. C., Salzer, J. J., Impey, C., Thuan, T. X., & Gronwall, C. 2002, *AJ*, 124, 3088
 Melbourne, J., Phillips, A. C., Salzer, J. J., Gronwall, C., & Sarajedini, V. L. 2003, in preparation
 Moshir, M., Kopman, G., & Conrow, T. A. O. 1992, *IRAS Faint Source Survey Explanatory Supplement, Version 2* (Pasadena: IPAC)
 Osterbrock, D. E. 1989, *Astrophysics of Gaseous Nebulae and Active Galactic Nuclei* (Mill Valley: Univ. Sci.)
 Salzer, J. J., Gronwall, C., Jangren, A., & McKinstry, K. 2003, in preparation
 Salzer, J. J., et al. 2000, *AJ*, 120, 80 (Paper I)
 ———. 2001, *AJ*, 121, 66 (KR1)
 ———. 2002, *AJ*, 123, 1292 (KB1)
 Stevenson, S., Salzer, J. J., Sarajedini, V. L., & Moran, E. C. 2002, *AJ*, 124, 3465
 Thorstensen, J. R., Wegner, G. A., Hamwey, R., Boley, F., Geller, M. J., Juchra, J. P., Kurtz, M. J., & McMahan, R. K. 1989, *AJ*, 98, 1143
 Van Duyne, J., Beckerman, E., Salzer, J. J., Gronwall, C., Thuan, T. X., Condon, J. J., & Frattare, L. M. 2003, in preparation
 Veilleux, S., & Osterbrock, D. E. 1987, *ApJS*, 63, 295
 Voges, W., et al. 1999, *A&A*, 349, 389
 Wegner, G., et al. 2001, *AJ*, 122, 2893
 White, R. L., Becker, R. H., Helfand, D. J., & Gregg, M. D. 1997, *ApJ*, 475, 479